



NATIONAL UNIVERSITY OF SCIENCE AND TECHNOLOGY POLITEHNICA BUCHAREST  
PhD School of Chemical Engineering and Biotechnologies

# Inorganic Materials with Luminescent Properties

**Liviu Dudaș**

A thesis submitted for the degree of  
**Doctor of Philosophy**

**Short Version**

Under the Advisorship of:  
**Professor Daniela-Cristina Berger**

2024

## Keywords

Oxidic ceramics, Rare Earths, Er<sup>3+</sup>, Yb<sup>3+</sup>, Upconversion, NIR illumination, 980 nm.

## Table of contents (shortened)

Chapter name	Page number
<a href="#">A0</a> Purpose and Objectives	2
<a href="#">A1a</a> Literature: Survey on luminescent inorganic materials	2
<a href="#">A1b</a> Literature: State of the art on photoluminescent oxide materials	3
<a href="#">A2</a> Concepts: Rare Earths.	4
<a href="#">A3</a> Concepts: Luminescence of Lanthanides	5
<a href="#">A4</a> Concepts: Upconversion Luminescence	6
<a href="#">A5</a> Methods: Syntheses of the Oxidic Ceramics	7
<a href="#">A6</a> Methods: Characterization of the Samples	9
<a href="#">A7</a> Possible and practical applications feasible in laboratory.	9
<a href="#">A8</a> Studied compositions, methods of synthesis, targeted aspects	10
<a href="#">B0</a> Summary of the articles (Original contributions)	11
<a href="#">C</a> Conclusions, accents on the results obtained, comparisons	14
<a href="#">D</a> Personal contributions	17
<a href="#">E</a> References (shortened)	18

## Introduction to the summary of the thesis

The kind of materials specified in the title of the work (inorganic materials) form a very broad category, yet this generality was restrained, due to the synthesis possibilities, to a few oxidic ceramics, which were more accessible to produce in the laboratory.

Also, the kind of luminescence studied was restrained to the one generated by the  $\text{Er}^{3+}$  ions when upconverting the incident 980 nm range radiation into the visible spectrum.

So, the work focuses on the synthesis, characterization, and emission spectra measurements of oxidic crystalline ceramic hosts in which the main metallic ions are from the lanthanide series, these being substituted by Er and Yb in sufficiently small concentrations as not to hinder the main crystalline phase.

The metals of substitution were Y, Gd, and La, and the oxidic compounds were  $\text{Y}_2\text{O}_3$ ,  $\text{BaGd}_2\text{ZnO}_5$ ,  $\text{BaY}_2\text{ZnO}_5$ ,  $\text{BaLa}_2\text{ZnO}_5$ , and  $\text{Y}_2\text{TiO}_5$ .

The thesis is structured as a short presentation for anybody who wants to delve into the study of the rare-earth elements luminescence as dopants in various crystalline hosts, and it has three parts.

The first part, chapters A1-A7, deals with the literature, concepts used, methods of synthesis, structural characterization of the oxidic ceramics, and the method for measuring the upconversion spectra.

The first chapters, A1a A1b, contain literature reviews for studies dealing with luminescent inorganic compounds with accents on the oxidic ceramics. Chapter A2 presents some generalities about the elements used for their luminescent properties: the rare earths. Chapters A3 and A4 speak about the luminescence of the lanthanides, presenting the main energy transfer types and the mechanisms involved in the upconversion.

The chapters A5 and A6 describe the general methods of the synthesis for the luminescent ceramics while chapter A7 gives some examples of the general practical applications of their luminescence. Chapter A8 gives indications about some practical applications which are quickly feasible in the laboratory in order to prove the economic value of the research.

The second part of the thesis, chapters B1 to B6, presents the results of the research organized as a list of articles, either published in ISI journals or in a preprint form.

The third part, last chapters (C, D), are about the conclusions and perspectives and emphasize the personal contributions. A list of some relevant references (chapter E) ends the work.

## Justification for choosing the thematic

The main justification of the thesis thematics is the gathering of knowledge regarding the luminescence of lanthanide ions when embedded in oxidic compounds.

This knowledge has two main directions: the first is the synthesis of the oxidic compounds, either powders or ceramics; the second is the study of the upconversion of the cheap and ready-available light, like 980 nm, into the visible range with the help of lanthanide ions, mainly  $\text{Er}^{3+}$  sensitized by  $\text{Yb}^{3+}$ .

Having such knowledge is very important due to the fact that the applications of it are very broad, starting from phosphors of all sorts (display panels or light sources), to nanoscale in vivo medical imaging, temperature sensors, drug delivery, to photovoltaic enhancers that gather, from the incoming sunlight, a much wider spectrum than that which today is used.

As such, the thesis objectives were the following:

- Mastering the synthesis and characterization of the oxidic compounds, powders, or crystalline ceramics, which act as embedding matrices for the rare-earth ions.
- Study the luminescence of the lanthanides as dopants in the above ceramics and understand the intimate mechanisms of
  - ✓ the internal energy transfers, intra-ionic, and between ions involved or with the lattice,
  - ✓ the crystal field splittings, temperature dependence,
  - ✓ controlling the color composition (visible spectrum components) of the resulted emissions
  - ✓ stability in time of the compounds.

The following pages are a summary of the thesis, from which the absolute relevant information was extracted. For the detailed information, I kindly ask the reader to refer to the full text.

## (A0) Purpose and objectives

### *Purpose of this work (IA-A1)*

This study aimed to understand synthesis methods and properties of inorganic materials, with a focus on accessible and economically feasible targets due to its complexity..

The study focused on metallic oxides doped with rare earths and oxidic ceramic synthesis methods, comparing results and efficiencies. Er<sup>3+</sup> ions were chosen for luminescence in upconverting 980 nm laser light. Er<sup>3+</sup> ions, commonly used as activators, are studied as single dopants or in combination with Yb<sup>3+</sup> ions, but their energetic interactions remain poorly understood.

The study aimed to enhance the efficiency of luminescence in doped oxidic ceramics by finding the cheapest and easiest method, while also understanding energy transfer mechanisms. After mastering oxidic host synthesis, extensive efforts were made to understand the energetic interactions between activators, sensitizers, and the host matrix of embedding. The research, still in its early stages, yielded significant results, paving the way for further exploration for more efficient compound preparation and practical applications..

### *Objectives of this work*

**Objective 1.** Nonconventional methods were used to obtain complex oxidic systems doped with Er<sup>3+</sup> and Yb<sup>3+</sup>, characterized from microstructural perspectives, and tested for ceramics under various sintering conditions..

**Objective 2.** The examination the luminescent properties of oxidic systems, focusing on upconversion signals for NIR light, removing LaPO<sub>4</sub> and CaGd<sub>2</sub>ZnO<sub>5</sub> due to poor efficiency..

**Objective 3.** The comparison the upconversion emission of ytterbium-sensitized erbium in various crystalline oxide matrices, focusing on efficiencies and minimizing total dopant concentrations to avoid structural changes in host matrices..

**Objective 4.** Gaining insight into the behavior and energy transfer mechanisms during the conversion of incident NIR light into visible radiation.

## (A1) Literature: Survey on luminescent inorganic materials

The chapter presents a comprehensive general literature survey, highlighting the latest trends and data for further research, despite the complexity of the task due to extensive research over decades.

### *General introduction*

As an example, one can start with the excellent review of Zheng et al. [1], where one can find not only general information about rare-earths, but also tables listing the synthesis and doping materials involved in rare-earth-doped inorganic nanomaterials research and applications.

The article discusses the development of nanomaterials with multi-disciplinary applications in bioimaging, therapy, drug delivery, neuroscience, sensing, detection, catalysis, light emission, information storage, encryption, nanolasing, and optical communication. It highlights challenges in controlling nanostructured architectures, modulating crystal size, morphology, and surface functionality, and using quantum mechanical simulations and machine learning..

Zhou et al. [2] review discusses organic materials for upconverting nano-particles (UCNP), with future research focusing on optimizing photostability, developing NIR-emissive triplet-triplet annihilation (TTA) based materials, and investigating nanotoxicity of lanthanide UCNPs..

### *Medicine applications*

For the use of upconversion luminescence in medicine, Bian et al. [3] reported about advancements in tumour phototherapy and UCNPs design and explain how the upconversion luminescent materials offer advantages in phototherapy by combining targeted and photosensitive drugs with unique optical properties of UCNPs;

For the cancer therapies, Xu et al. [4] developed biodegradable Cu/Mn silicate nanospheres coated with lanthanide-doped nanoparticles for trimodal imaging-guided synergistic therapy.

Shwetabh et al. [5] studied polyethylene glycol-coated hexagonal phase nanoparticles of NaGdF<sub>4</sub>:Tm<sup>3+</sup>/Yb<sup>3+</sup> and showed that the photo-thermal conversion efficiency could be used for cancer treatment being good in situ temperature sensing.

### *Thermometry in bioapplications*

A study about nano-thermometers for bio-applications was done by Jurga et al. [6] They gave a list of Nd<sup>3+</sup>-doped UC nanoparticles used for bio-thermometry and also indicated the design of nano-thermometers with optimal excitation and emission wavelengths, showing that they could detect emissions from deeper tissues beyond reported ranges. Many compositions of rare earth doped UCNPs were described.

### *Imaging and drug delivery*

For in vivo drug delivery, Li et al. [7] developed nanospheres for imaging and anti-cancer drug delivery; they produced uniform, monodisperse, and core-shell nanospheres made of mesoporous silica-coated individual nanoparticles.

For in vivo imaging, Maji et al. [8] used UCNP as inclusion complexes with  $\alpha$ -cyclodextrin in vivo bioimaging.

Photodynamic therapy was performed by Chatterjee [9] by realizing monodisperse UCNPs associated with tumor antigens.

#### *Photovoltaic conversion enhancement*

The application of UC in photovoltaic enhancement is a topic of interest, so Ju & Li [10] presented a comprehensive review in which they analysed applications of upconversion, downconversion, and luminescent down-shifting technologies in solar cells.

Specifically, Ju & Li discussed the upconversion technology used in thin-film solar cells, perovskite cells, dye-sensitized cells, and quantum-dot-sensitized solar cells. Er<sup>3+</sup> doping in the NaYF<sub>4</sub> matrix as an upconversion layer shows that its emission band ranges from 523 nm to 669 nm, green to red light, and excitation band from 800 nm to 1550 nm.

#### *Piezoelectric materials*

Chen et al. in [11] made an extensive review in which they compared various RE doped piezoelectric materials and pointed toward development of lead-free ceramics with large strain and high energy conversion.

#### *Thermometry in industry*

Shang et al. [12] showed that Li doped Er, Yb silicate films can be used in thermometry for a temperature range of 80 - 460 K. Lee et al. [13] studied K<sub>5</sub>Y(P<sub>2</sub>O<sub>7</sub>)<sub>2</sub> doped with Er and Yb for its thermometric properties noting excellent sensitivity of 1.01%/K at 293. Liu et al. [14] obtained Ba<sub>3</sub>Y<sub>4</sub>O<sub>9</sub>:Er:Yb phosphors through solid-state reaction method. Li and Zhu [15], showed how core-shell Tm@Yb@Er phosphors can manipulate upconversion. Wang et al. [16] synthesized Ba<sub>5</sub>Zn<sub>4</sub>Y<sub>8</sub>O<sub>21</sub>-based phosphors and showed improved emission color and temperature-sensing performance. Wang et al. [17] synthesized Y<sub>2</sub>O<sub>3</sub>: 5%Yb<sup>3+</sup>, 0.5%Tm<sup>3+</sup>, z%Ho<sup>3+</sup> samples using a CO<sub>2</sub> laser zone melting method, a low-cost process.

#### *Phosphors for displays*

Yang et al. [18] synthesized Lu<sub>2</sub>O<sub>3</sub>:Yb,Tm,Er nanocrystals and study the energy transfers from Yb ions to Tm and Er via ground and excited states absorptions. Etchart et al. [19], found UC efficiencies of 5% at room temperature for BaY<sub>2</sub>ZnO<sub>5</sub>:Yb,Er and BaGd<sub>2</sub>ZnO<sub>5</sub>:Er,Yb which are higher than that of NaYF<sub>4</sub>:Yb,Er. Zhou et al. [20], showed how lanthanide-doped UCNPs exhibit cross-relaxation and efficient energy transfer upconversion. Drizdowski et al. [21] synthesized persistent luminescence phosphors with upconverting LiYbF<sub>4</sub>:Tm<sup>3+</sup>@LiYF<sub>4</sub> core-shell nanoparticles exhibiting dual-modal behavior. Zhu et al. [22] produced NaYF<sub>4</sub>:Er,Ho nanocrystals with core-shell structure made from achieving pure red emission under 1550 nm excitation finding the shift toward yellow at increasing the power of 980 nm incident light.

#### *Energy transfer mechanisms*

Berry and May [23] discussed the mechanism by which incident NIR is transformed to visible red by Er<sup>3+</sup> as dopant in NaYF<sub>4</sub>. Yin et al. [24] used gold nanorods (AuNR) on PMMA Opal Photonic Crystals. Liu et al. [25] synthesized optical-magnetic bifunctional NaGdF<sub>4</sub>:Er,Yb. Vetrone et al. [26] discussed the red shift of the UC emission of Er<sup>3+</sup> doping Y<sub>2</sub>O<sub>3</sub> when the Yb<sup>3+</sup> concentration increase. Rivera-Lopez et al. [27] synthesized YBO<sub>3</sub>:Yb,Er phosphors by solid-state.

## **(A1) Literature: State of the art on photoluminescent oxide materials**

This chapter provides an overview of recent literature on luminescent oxidic compounds, comparing objectives, methods, compounds, and research aspects with those in specialized literature, demonstrating clear integration.

Hu et al. [28] prepared KYb(MoO<sub>4</sub>)<sub>2</sub>: 0.1%. Er<sup>3+</sup> self-activated phosphors utilizing a high-temperature solid-state reaction (HT-SSR) technique.

Wang et al. [29] prepared Er<sup>3+</sup>-doped Y(Nb,Ta,V,P)O<sub>4</sub> phosphors successfully prepared using HT-SSR method.

Sarkar et al. [30] prepared Er<sup>3+</sup>/Yb<sup>3+</sup> doped YVO<sub>4</sub> and GdVO<sub>4</sub> phosphores and found that both types of compounds samples had good upconversion.

Du et al. [31] studied the multimodal and multicolor luminescence in CaWO<sub>4</sub>:Yb<sup>3+</sup>,Er<sup>3+</sup>,Eu<sup>3+</sup> phosphors by using traps and rare earth emissive centers for emission control.

Zhang et al. [32] studied multifunctional photon conversion materials for silicon solar cells (SSC) and presented for the first time NaY(WO<sub>4</sub>)<sub>2</sub>:Er<sup>3+</sup>,Yb<sup>3+</sup> which combines upconverting, quantum-cutting, and temperature sensing to improve SSC performance.

Makumbane et al. [33] deposited thin films of Y<sub>2-x-y</sub>O<sub>3</sub>:Ho<sub>x=0.005</sub>,Yb<sub>y=0.05</sub> on soda-lime glass substrates using pulsed laser deposition (PLD) technique.

Jin et al. [34] fabricated Ho<sup>3+</sup>-doped Yb<sub>2</sub>W<sub>3</sub>O<sub>12</sub> phosphors using the solid-state technique noting that the doping content had no substantial effect on the Yb<sub>2</sub>W<sub>3</sub>O<sub>12</sub> phase.

De et al. [35] prepared BaWO<sub>4</sub>:Yb,Er nanophosphor using the hydrothermal method, they recorded the green and red emissions of Er<sup>3+</sup> transitions and tuned Er<sup>3+</sup> concentration for maximum fluorescence intensity at 3% and for Yb<sup>3+</sup> at 5%.

Borges et al. [36] prepared Ta<sub>2</sub>O<sub>5</sub>:Er<sup>3+</sup>,Yb<sup>3+</sup> nanoparticles by firstly treating tantalum ethoxide in ethylene glycol to form a stable tantalum precursor and mixed it in acetone and by this they controlled the morphology and size of the precursor particles at 164 to 302 nm .



Hu et al. [37] prepared for the first time  $\text{Yb}^{3+}, \text{Er}^{3+}$  co-doped  $\text{Ba}_3\text{Sc}_2\text{WO}_9$  nanophosphor for red UC luminescence. They found that the optimal doping concentrations are 10% for  $\text{Yb}^{3+}$  and 3% for  $\text{Er}^{3+}$ , with red-green intensity ratios up to 23.06.

Hu et al. [38] also prepared  $\text{Sc}_6\text{WO}_{12}:\text{Yb}^{3+}, \text{Er}^{3+}$  phosphor for bright red UC luminescence when excited with a 980 nm near-infrared laser.

Jung et al. [39] used spray pyrolysis technique to produce spherical particles of  $(\text{Ti}_{1-x}\text{Si}_x)\text{O}_2:\text{Er}, \text{Yb}$  phosphors. They demonstrated by XRD and FTIR examination that the inclusion of Si improves thermal stability.

Singh et al. [40] synthesized  $\text{Er}^{3+}$  doped and  $\text{Er}^{3+}, \text{Yb}^{3+}$  co-doped  $\text{CaTiO}_3$  phosphors using SSR at 1473 K. They showed that phosphores have an orthorhombic phase in the  $\text{Pnma-62}$  space group and the crystallites and particle size grow in the presence of  $\text{Er}^{3+}$  and  $\text{Yb}^{3+}$  ions.

Jiang et al. [41] synthesized monodisperse  $\text{Y}_2\text{O}_3$  phosphors utilizing a homogeneous precipitation technique.

Roy et al. [42] produced, using SSR method,  $\text{Y}(\text{Vn}, \text{Nb}, \text{Ta})\text{O}_4$  doped with  $\text{Ho}^{3+}$  and  $\text{Yb}^{3+}$  with the combinations  $\text{YTa}_{1-0.25}\text{V}_{0.25}\text{O}_4$ ,  $\text{YTa}_{1-0.5}\text{Nb}_{0.5}\text{O}_4$ , and  $\text{YNb}_{1-0.75}\text{V}_{0.75}\text{O}_4$ . They observed how  $\text{YVO}_4:\text{Ho}^{3+}:\text{Yb}^{3+}$  and  $\text{YNbO}_4:\text{Ho}^{3+}:\text{Yb}^{3+}$  crystallize as pure phases while  $\text{YTaO}_4:\text{Ho}^{3+}:\text{Yb}^{3+}$  shows impurity peaks due to  $\text{YTa}_7\text{O}_{19}$ .

Singh et al. [43] synthesized  $\text{CaMoO}_4:\text{Er}^{3+}, \text{Yb}^{3+}$  phosphor co-doped with  $\text{Bi}^{3+}$  ions and found that the UC luminosity is enhanced by  $\text{Bi}^{3+}$  co-doping. They noted that the general tetragonal structure of  $\text{CaMoO}_4$  is maintained but local distortions are produced and that the UC emission is enhanced by the asymmetry surrounding  $\text{Er}^{3+}$  ions.

Singh et al [44] prepared  $\text{CaTiO}_3$  based phosphor by SSR at 1473 K and doped it with  $\text{Sm}^{3+}$  and co-doped it with  $\text{Li}^+, \text{K}^+, \text{Mg}^{2+}, \text{Ba}^{2+}, \text{Gd}^{3+}, \text{Bi}^{3+}$ . They observed, using XRD and SEM, that the order  $\text{Li}^+, \text{Mg}^{2+}, \text{Gd}^{3+}, \text{K}^+, \text{Bi}^{3+}, \text{Ba}^{2+}$  is the order in which these moderators cause the crystallite and particle sizes to decrease.

Dutta et al [45], by using SSR method, synthesized  $\text{Zn}_2\text{TiO}_4:\text{Yb}^{3+}, \text{Tm}^{3+}$  and found that the incompatible ionic radii cause lattice strain, which alters the average crystallite size and that 145.66 nm was the average particle size determined by HR-TEM analysis.

Cheng et al. [46] propose a model of energy transfers between activators and sensitizers called "energy migration upconversion" model (EMU). They show that the EMU procedure eliminates the need for activators with ladder-like energy levels and EMU approach enables photon upconversion for several lanthanide ions simultaneously.

## (A2) Concepts: Rare Earths

### *Generalities and properties of rare earths*

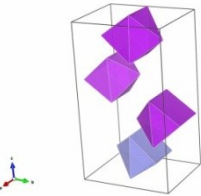
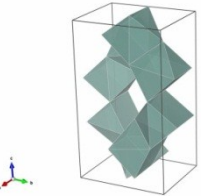
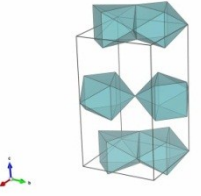
Rare earth elements (RE) belong to the Lanthanides group of the periodic table, along with scandium and yttrium, found in the same minerals as lanthanides. Rare earth properties are crucial in modern technology, used in various applications such as electrical engines, display panels, fiber optics, batteries, ceramics, optical glasses, and X-ray phosphors. Rare minerals contain low concentrations of these elements, making extraction costly and rarely a byproduct of more profitable processes like thorium, titanium, or bauxite.

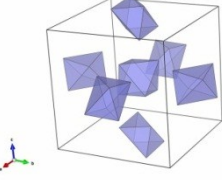
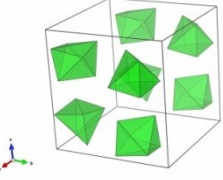
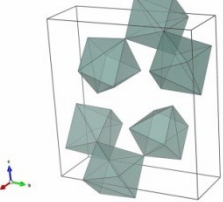
Lanthanides, rare earths with an open 4f shell, are chemically similar and primarily trivalent, with tetravalent (Cerium, Praseodymium, Terbium) and divalent (Samarium, Europium, Ytterbium) being the most important. A 4f shell, having many electrons, also has a big number of quantum states, so that the number of energy levels for an electronic configuration is large. E.g., for  $\text{Er}^{3+}$  with  $4f^{11}$ , one has 17 LS terms, 41 energy levels, but  $\text{Gd}^{3+}$  has 119 LS terms and 327 energy levels.

### *Crystalline rare-earths oxidic compounds*

The research focuses on oxidic compounds of Y, Gd, and La doped with Er and Yb, examining how these compounds accept the host matrix's coordination polyhedron and point symmetry. The point group of symmetries of a site significantly influences the energy transition probabilities of an ion, as the final electronic configurations must align with the point group's irreducible representations. In Table A2.1 are presented the unit cells of the crystalline oxides we've studied.

**Table A2.1.** Examples of coordination polyhedra. For clarity, only some of them are shown for a unit cell. The oxide formula, the crystal group, the form of the polyhedron, the substituted ion coordination number and the point group are specified.

		
<p>• <math>\text{BaGd}_2\text{ZnO}_5</math>: substituted: <math>\text{Gd}^{3+}</math></p>	<p>• <math>\text{BaY}_2\text{ZnO}_5</math>: substituted <math>\text{Y}^{3+}</math></p>	<p>• <math>\text{BaLa}_2\text{ZnO}_5</math>: substituted <math>\text{La}^{3+}</math></p>

<ul style="list-style-type: none"> <li>• Pnma-62 (orthorhombic)</li> <li>• Square pyramid attached to a 3-prism.</li> <li>• Coordination VII: all sites</li> <li>• Point group is <math>C_{2v}</math>: all sites</li> </ul>	<ul style="list-style-type: none"> <li>• Pnma-62 (orthorhombic)</li> <li>• Square pyramid attached to a 3-prism.</li> <li>• Coordination VII: all sites</li> <li>• Point group is <math>C_{2v}</math>: all sites</li> </ul>	<ul style="list-style-type: none"> <li>• I4/mcm (tetragonal)</li> <li>• Two square pyramids attached to a 3-prism.</li> <li>• Coordination VIII: all sites</li> <li>• Point group is <math>C_{2v}</math>: all sites</li> </ul>
		
<ul style="list-style-type: none"> <li>• <math>Y_2O_3</math>. substituted: <math>Y^{3+}</math>- optic inactive sites</li> <li>• Ia-3 (cubic)</li> <li>• Two parallel antisymmetrical equilateral triangles with edges to the closest point.</li> <li>• Coordination VI: all sites</li> <li>• Point group is <math>C_{3i}</math>: 1/4 of all sites</li> </ul>	<ul style="list-style-type: none"> <li>• <math>Y_2O_3</math>: substituted: <math>Y^{3+}</math>- optic active sites</li> <li>• Ia-3 (cubic)</li> <li>• Two tilted 4 pyramids symmetrically attached to a common trapezoid bottom</li> <li>• Coordination VI: all sites</li> <li>• Point group is <math>C_{2v}</math>: 3/4 of all sites</li> </ul>	<ul style="list-style-type: none"> <li>• <math>Y_2TiO_5</math>: substituted <math>Y^{3+}</math></li> <li>• Fd-3m (cubic)</li> <li>• An irregular 9-hedron.</li> <li>• Coordination VIII: all sites</li> <li>• Point group: <math>C_1</math></li> </ul>

### *Point group vs. crystal group, crystal radii, ionic radii, oxidation states*

A distinction must always be made: the symmetry group of the crystal is different from the point group of the coordination polyhedra. In a crystal, the J multiplet of the energy levels of the ion is split by the electric crystal field (Stark effect). As an example, from **Table A2.1**, we see that the main point group of the optical active sites in the crystals that we characterized is  $C_{2v}$ , which has the irreps A1, A2, B1, B2. We studied the spectra of  $Er^{3+}$ , which has 11 electrons in the 4f shell being a non-integer total J ion, the ground state having  $J=15/2$ . It is mandatory to take into consideration the ionic or crystal radii of the ions when synthesizing and inserting dopants in the different oxides. Because of the differences between these radii, the substitutions of the dopant ions could give rise to crystalline matrix defects. **Table A2.2** shows the ionic radii for  $Er^{3+}$  and  $Yb^{3+}$ .

Ion	Coordination	Crystal Radius	Ionic Radius
$Er^{3+}$	VI	1.030	0.890
	VII	1.085	0.945
	VIII	1.144	1.004
$Yb^{3+}$	VI	1.008	0.868
	VII	1.065	0.925
	VIII	1.125	0.985

## (A3) Concepts: Luminescence of Lanthanides

### *Types of luminescence*

Lanthanide ion luminescence is influenced by the surrounding environment of the ion. Gaseous phases have sharp spectral lines with a precision of  $0.01 \text{ cm}^{-1}$ . Liquid phases cause widening spectra and absorption, while solid environments, like crystalline or amorphous glasses, strongly influence spectra.

### *Energy transitions of lanthanides in solids (radiative and non-radiative)*

A radiative transition in a solid occurs when the gap between the two energy levels exceeds at least four to five phonon energies. Non-radiative decay involves two steps: exciting a phonon into a promoter mode and losing energy into other modes, with multiphonon decay rate directly proportional to mode probability. The coupling with lattice parameters of electronic states E1 and E2 influences multi-phonon transition probabilities, with increased occupation numbers for phonon modes affected by temperature. Knowing the maximum phonon energy is crucial for designing luminescence efficiency, as a small energy difference  $\Delta E$  leads to fast decay with direct phonon emission. The transfer of energy to a high-energy phonon mode, typically optical, results in rapid thermalization due to spreading on other modes, resulting in weak phononic anti-Stokes bands.

### *Luminescent transitions types*

The luminescence intensity and line broadening are dependent on the type of electronic transition generating it, types of which are presented below.

The parity rules for free ions typically prohibit  $4f^n \rightarrow 4f^n$  intraconfigurational transitions, but when embedded in solids, the parity symmetry is broken, allowing forced electric dipole type transitions. The initial and final wavefunctions are a mixture of configurations  $4f^n$  and  $4f^{n-1}5d$ , with strength typically 3-4 orders of magnitude weaker than fully allowed electric dipole one. The transitions in ion sites with inversion symmetry require coupling wavefunctions with odd vibronic modes' symmetries, as this cancels out the odd parity of the electric dipole operator. Band-to-band transitions occur when an electron is excited into the conduction band, transferring energy to the ion, which fluoresces due to the overlapping with the upper levels of the lanthanide ion. The interconfigurational ( $4f^n \leftrightarrow 4f^{n-1}5d$ ) transitions, which present also broadening effects due to the complexity of the interactions, vibronic interactions being involved. Charge-transfer transitions occur when  $Ln^{3+}$  receives an electron from the

ligand cloud, creating a hole, and changes to  $\text{Ln}^{2+}$ , resulting in a high-energy vibrational state and widened emission. Transitions that occur due to  $\text{Ln}^{3+}$  embedding in unique sites, such as interfaces, segregation zones, structurally different phases, or surface interactions with hydroxyl ions. These transitions, with their distinct features, are crucial in assessing the purity of a compound as they serve as signatures of defects or impurities.

## (A4) Concepts: Upconversion luminescence

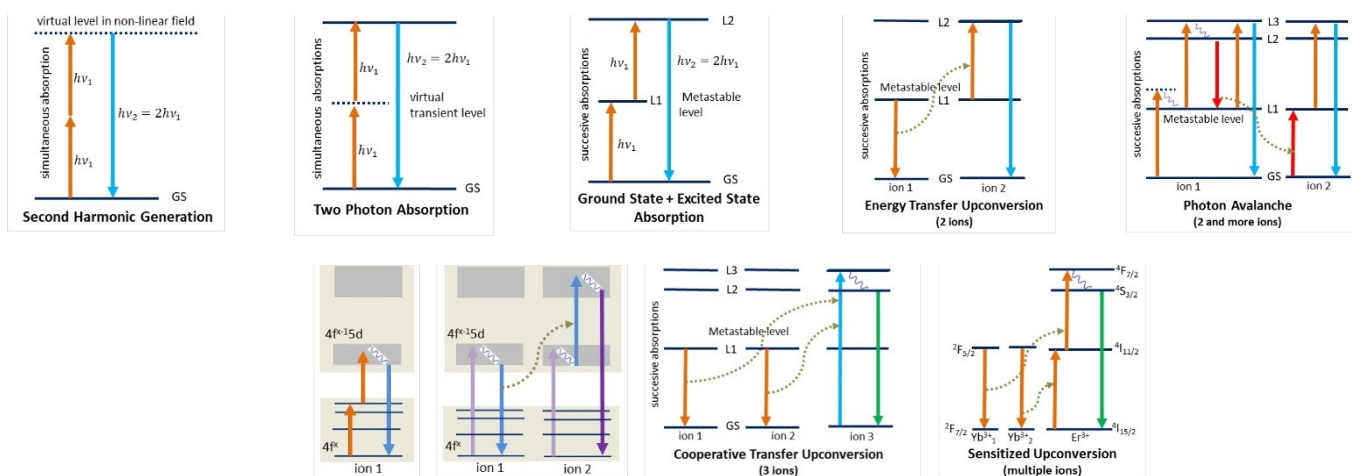
### Definition

Upconversion (UC) is the process where a system with multiple metastable energy levels absorbs photonic or phononic energy, jumps through absorption events, and de-excites to a lower state with higher energy quanta. The process requires selecting  $\text{Ln}^{3+}$  with stable energy levels that prevent decay before absorption of photons or phonons, allowing the ion's energy to increase steadily.

It is important to choose an appropriate host matrix of embedding the  $\text{Ln}^{3+}$  ion, which should not facilitate the undesired nonradiative decays.

### Mechanisms

The upconversion processes are realized through several mechanisms from which I present the most important ones:



**Second harmonic generation (SHG)** generates photons with double energy than those absorbed. **Two or multi-photon absorption (TPA/MPA)** is when two photons from the laser field are absorbed via a virtual, transient state. **Ground state + excited state absorption (GSA+ESA)** implies the extraction of two photons from the laser field in quick successful events. **Energy transfer upconversion (ETU)** involves two ions with cross-relaxation energy transfer. All the two photon processes aforementioned, TPA, GSA+ESA, and ETU, are easily detectable by plotting the log-log correlation of the measured emission intensity vs. the power of the laser. A factor around 2 is an indication of a two-photon process. **Photon avalanche (PA)** is better explained through the image and involves few steps: a) a photon  $h\nu$  is nonresonantly absorbed by the first ion which jumps from GS to L1, the energy difference ( $h\nu - E_B$ ) being absorbed into lattice, b) the first ion, being in the state L1, absorbs a second photon jumping to state L3, c) the first ion decays to L2 non radiatively, d) cross relaxation takes place between the first and the second ions both reaching the state L1. e) both ions perform ESA and decay to GS by stimulated emission. **Cooperative energy transfer (CET)** involves two ions which, when decaying simultaneously, transfers the energy to a third which jumps to a level whose energy is the sum of the emitted virtual photons. **4f-4f  $\rightarrow$  4f-5d upconversion** can be done involving 4f-5d configurations through successive photon absorption can push the energy level into the 4f-5d bands from where the decays are either to ground or some cross-relaxation pushing other ions also in 4f-5d band. **Sensitized upconversion**, when the presence of  $\text{Yb}^{3+}$  facilitates the transition of  $\text{Er}^{3+}$  to higher levels because  $\text{Yb}^{3+}$  absorbs very well the 976 nm radiation through the transition  $^4F_{5/2} \leftarrow ^4F_{7/2}$  and transfers it to  $\text{Er}^{3+}$ , either as one to one cross relaxation or two ions transfer from a pair of  $\text{Yb}^{3+}$  to one  $\text{Er}^{3+}$  which jumps directly to  $^4F_{7/2}$ .

### General applications of the upconversion

**Phosphors** for fluorescence lamps, the colors are easy tunable because RE ions transitions, having a great color gamut, one can choose the RE ions which gives the desired color hues. Examples of compounds are  $\text{Y}_6\text{WO}_{12}:\text{Yb}^{3+}/\text{Er}^{3+}$ ,  $\text{NaYF}_4:\text{Ho}^{3+}, \text{Yb}^{3+}$ ,  $\text{BaCl}_2:\text{Er}^{3+}$ ,  $(\text{Ba}, \text{Sr})_2\text{Si}_5\text{N}_8:\text{Eu}^{2+}$  and  $(\text{Ca}, \text{Sr})\text{AlSi}_3\text{N}_3:\text{Eu}^{2+}$ .

**Quantum cutting** by which a photon with large energy is absorbed, putting the ion in a state of high energy and the decay to ground is performed in a single event through emission of two or more photons, each of them with a lower energy than that of the one absorbed. Examples of compounds used



are: Tm/Tb/Pr and Yb co-doped oxide phosphors, (Tm<sup>3+</sup>, Yb<sup>3+</sup>) and Bi<sup>3+</sup> activated GdNbO<sub>4</sub> or Tm<sup>3+</sup>/Yb<sup>3+</sup> co-doped Y<sub>2</sub>O<sub>3</sub>.

*Flat panel detectors* in which the lanthanide phosphors are excited by micro electron guns. Examples of compounds are: Gd-based thin films.

*Plasma displays* in which the Ln<sup>3+</sup> doped phosphors excited by plasma generated by inert gas discharges; examples are: YAG:Eu<sup>3+</sup>, YAG:Tb<sup>3+</sup> and BAM:Eu<sup>2+</sup>, (Y,GD) BO<sub>3</sub>:Eu<sup>3+</sup>/NaLa(PO<sub>3</sub>)<sub>4</sub>:Tb<sup>3+</sup>:Eu<sup>3+</sup>.

*In the medical field* to name just a few applications like DNA computing, lymphatic imaging, cancer cells imaging, in situ NIR light controlled drug delivery, detection and labeling pathogenic bacteria etc. Examples are: tetramethylbenzidine linked to UCNPs, oleic acid capped NaLuF<sub>4</sub>:Yb,Tm, NaYF<sub>4</sub>:Y:Er oleate UCNPs + 4D5 scFv-Bn protein, NaYF<sub>4</sub>: Yb,Er@NaYF<sub>4</sub>:Nd,Yb UCNPs on organic photovoltaic, NaYF<sub>4</sub>:Yb,Er UCNPs attached to oligonucleotide magnetic nanoparticles, NaYF<sub>4</sub>:Yb/Er@SiO<sub>2</sub>@mesoporous SiO<sub>2</sub>-Ca.

Luminescent nanoparticles which are used for high-definition imaging (under microscope) or bio labeling. Examples are: NaYF<sub>4</sub>:Yb,Er@NaYF<sub>4</sub> UCNPs functionalized with NH<sub>2</sub>, tetrazine or foling acid, BaGdF<sub>5</sub>:Yb/Er with polyethylene glycol, (NaYF<sub>4</sub>:Yb30%,Tm0.5%, Nd5%)(NaYbF<sub>4</sub>)(NaYF<sub>4</sub>:Nd30%) + azobenzene + photoisomerization polymer, NaGdF<sub>4</sub>:Yb/Er@SiO<sub>2</sub>-NH<sub>2</sub> and mercaptopropionic acid + glutathione Ag<sub>2</sub>S nanodots, Yb/Tm co-doped NaYF<sub>4</sub>.

*Organic light emitting diodes.* Examples of compounds are: methyl-phenylpentene-dione:Er<sup>3+</sup>, allyl-oxo-butanoate:Er<sup>3+</sup>, tetrakis β-diketonates of La complexes, thienyl-trifluoroacetato-europium.

Scintillators for gamma rays, with high yield, examples are ZnO-TiO<sub>2</sub> upconversion scintillator containing Er<sup>3+</sup> and Yb<sup>3+</sup>[99], Y<sub>2</sub>O<sub>3</sub>:Yb(2%):Er(1%).

Photovoltaic panels efficiency enhancers, which try to bring into the absorption range of Si (1100 nm absorption) the energy bands which are either too energetic (so, use downconversion) or infrared (upconversion used); examples of compounds are: LiYF<sub>4</sub>:Yb<sup>3+</sup>,Er<sup>3+</sup>, Er<sup>3+</sup>:Yb<sup>3+</sup> doped vitroceraic for GaAs solar cells or Ba<sub>2</sub>F<sub>8</sub>:30%Er<sup>3+</sup> for Si solar cells, NaGdF<sub>4</sub>:Yb/Er, LaEr(MoO<sub>4</sub>)<sub>3</sub> or BaTiO<sub>3</sub>:Yb/Er.

Tunable nanodots in which the phonon dispersion is controlled by adjusting the particle dimensions and so the non radiative transitions of Ln<sup>3+</sup>. Examples are: GdOF:Yb<sup>3+</sup>/Er<sup>3+</sup>@(Au nanodots@bovine serum albumin)-doxorubicin-folic acid, NaYF<sub>4</sub>:Y78%:Yb20%:Er2%) with copolymers, Ln-Doped Gd<sub>2</sub>O<sub>3</sub>.

*Energy levels of Er<sup>3+</sup> and Yb<sup>3+</sup>*

Table A5.1 presents the values of the energies for the levels of the Er<sup>3+</sup> ion and the differences between them, expressed in cm<sup>-1</sup>.

Nr	Energy	Term	differences from level to those below cm-1							differences between levels cm-1							
			to 0	to 1	to 2	to 3	to 4 to virt 1	to 5	to 6	x to -1	x to -2	x to -3	x to -4	x to -5	x to -6	x to -7	
0	0	4i(15/2)	0														
1	6516	4i(13/2)	6516	0							6516						
2	10150	4i(11/2)	10150	3634	0						3634	10150					
3	12384	4i(9/2)	12384	5868	2234	0					2234	5868	12384				
4	15267	4F(9/2)	15267	8751	5117	2883	0				2883	5117	8751	15267			
	16762	Virtual 1	16762	10246	6612	4378	1495	0			1495	4378	6612	10246	16762		
5	18403	4S(3/2)	18403	11887	8253	6019	3136	1641	0		1641	3136	6019	8253	11887	18403	
6	19167	2H(11/2)	19167	12651	9017	6783	3900	2405	764	0	764	2405	3900	6783	9017	12651	19167
7	20516	4F(7/2)	20516	14000	10366	8132	5249	3754	2113	1349	1349	2113	3754	5249	8132	10366	14000
8	22200	4F(5/2)	22200	15684	12050	9816	6933	5438	3797	3033	1684	3033	3797	5438	6933	9816	12050
9	22519	4F(3/2)	22519	16003	12369	10135	7252	5757	4116	3352	319	2003	3352	4116	5757	7252	10135
10	24500	2H(9/2)	24500	17984	14350	12116	9233	7738	6097	5333	1981	2300	3984	5333	6097	7738	9233
	25900	Virtual 2	25900	19384	15750	13516	10633	9138	7497	6733	1400	3381	3700	5384	6733	7497	9138,1
	Excitation energy		980nm = 10200 cm-1														
	Thermal energy		300K = 209 cm-1														

## (A5) Methods: Synthesis of the Oxidic Ceramics

### *Synthesis methods of the oxides*

The synthesis method ensures uniform atomic level constituent mixing for desired crystal phase without segregations, stoichiometry changes, crystal defects, or dopant ion substitution. Below are presented several methods used for oxide powder synthesis.

#### **Solid state method**

The solid-state method consists of mixing the metallic oxides or carbonates in the appropriate stoichiometric ratios. Sometimes, a dispersion agent or an additive can be added for a better homogenization of the reaction mixture by grinding using a mortar or a ball mill. The milling or grinding of the solid-state mixture usually lasts several hours. A sieving step could be used to ensure the selection of particles with a narrow size distribution. An advantage of this method is its simplicity, but it is suitable only for oxidic systems, which are stable at high temperatures. The main drawback is related to the large energy consumption because usually it requires a high temperature and a long period of time because the kinetics of the chemical reaction between the solid-state reagents are very slow, as are the large particles that form..

#### **Combustion method**

The combustion method for the synthesis of oxidic nanomaterials, is based on an exothermic redox reaction between metallic nitrates that are oxidizing agents and an organic compound named fuel, usually a carboxylic acid, an aminoacid, or urea, which acts either as a reducing agent or chelating agent. The molar ratio in which the fuel must be added to the mixture of metallic nitrates is calculated

based on oxidizing/reducing valences used in propellant chemistry. When solid reactants are used, a high temperature for self-propagating reactions is reached. Even if this is an old technique (45 years) and it is used on an industrial scale, it implies high costs and has low efficiency.

#### Solvothermal method

This method is suitable for the cases in which a certain oxidic or salt crystalline phase is desired, and the parameters: temperature, duration, pH, and type of solvent (when water is used, the method is called hydrothermal, and when another solvent is the reaction medium, the method is called solvothermal) are tuned for obtaining the desired crystalline compound. Usually, metallic oxides are prepared from various salts dissolved in water, followed by metallic ion precipitation as corresponding hydroxides using a concentrated aqueous solution of the precipitating agent, followed by a hydrothermal/solvothermal treatment under autogenous pressure or an additional gas pressure (for instance, additional pressure of inert gas) using a reactor, which can be a Teflon/glass-lined stainless steel reactor. At the end of this process, the reactor is cooled down either suddenly or slowly, and then the compound formed as a precipitate of microcrystals is washed with deionized water, filtered off, and dried. This method is not appropriate for obtaining doped oxide powders because the crystallization of various oxides has different rates.

#### Coprecipitation method

The solutions containing the metallic salts (nitrates, acetates, etc.) are mixed under magnetic stirring, then a precipitating agent (usually ammonia, alkaline hydroxides) is poured dropwise under constant stirring until all metallic ions are precipitated as hydroxides or oxyhydroxides. Sometimes, to prevent particle aggregation, a surfactant could be added. Parameters that influence the structure and morphology of the resulting compound are the concentration of metallic salt and precipitation agent, pH temperature of the reaction mixture, etc. The method is simple, the temperatures are moderate, and the morphology can be controlled, and usually the calcination temperatures are lower than in the case of the solid-state method. However, sometimes it is difficult to control the stoichiometry during the precipitation step if there are several metallic ions in the system. To prevent accidental carbonation with the CO<sub>2</sub> from the air, the operations could be performed either in protective inert gas or at least in a closed atmosphere.

#### Thermal decomposition of complex precursors

One of the most known chelating agent for metallic ions, especially for alkaline-earth metals is ethylene-diamine-tetra-acetic acid (EDTA) being able to form complex compounds that thermally decompose at temperatures lower than 1000 °C. It is also used to extract metal ions from different environments, like contaminated soils, because of its capacity to form stable complex compounds.

#### Citrate - EDTA method

The citrate-EDTA method is considered a type of sol-gel method and is usually applied for obtaining complex oxidic systems in which either alkaline-earth metals or transition metals are. This method uses citric acid (CA) which is able to form stable chelates with transition metals and EDTA that forms complex compounds with alkaline-earth metals whose stability depends on the type of metallic ion.

#### Pechini method

Pechini method has been applied successfully to obtain many pure or doped oxidic systems. Pechini method is considered a type of sol-gel technique. In this method different metallic salts or metallic alkoxides dissolved in water, alcohol or even in ethylene glycol can be used. As complexation agent, citric acid is used because it can form stable chelates with several metallic ions. The third carboxylic group of citric acid is involved in the esterification reaction with ethylene glycol or other polyhydroxialcohol, which occurs at 130°-140°C with the formation of a polymeric-type precursor, in which the metallic ions are uniform distributed. The organic part is removed by a thermal treatment. A schematic of a general modified Pechini procedure is shown in **Figure A6.1**. This method allows to obtain oxide powders at lower temperatures than other methods, including doped oxide systems. This method is the most advantageous for what we needed because is flexible, the variety of the oxidic compounds obtained is large, various types of starting reagents can be used (nitrates, carbonates, chlorides etc.), ensures homogeneous distribution of metallic ions by chelation in a large pH domain. Nevertheless, the duration of process is long, and during the thermal treatment gases (some toxic) are evolved.

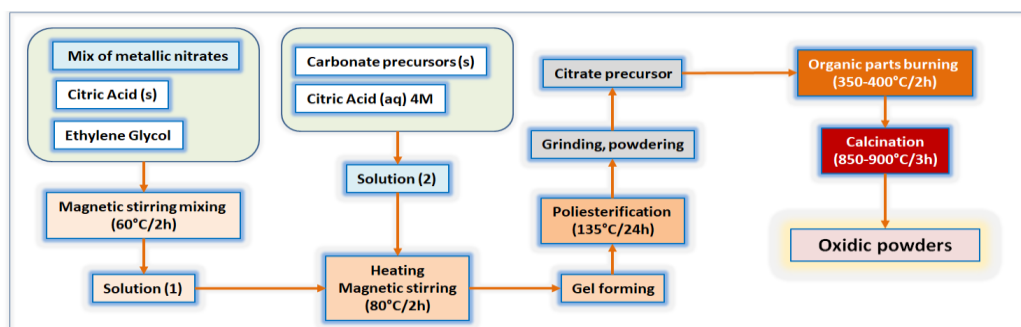


**Figure A6.1.** A schematic view of the work-flow for the modified Pechini method.

**Obtaining the ceramic pellets****Pressing the oxide powders**

The oxidic powders obtained through the above-described citrate sol-gel method were put into a 13 mm diameter steel die in successive 'add-a-bit, then press' steps in order to get rid of the air trapped between particles. The air trapped is always a nuisance and should be avoided totally since it induces cleavage and the pellet will break. The pellets were passed through the appropriate number of cycles of pressing and grinding until stable and well compacted pellets were formed. Great care was always taken not to contaminate the samples with residues from various sources. The pressing forces used were in the range of 100kN to 200kN. Usually, the first step of pressing was done at 200 kN for 2 minutes, then the resulting pellet was re-grinded and re-pressed at 100 kN for 1 minute, after which the result was satisfactory.

**Sintering of the oxidic pellets**

The conditions only allowed us for the conventional method of high temperature furnace treatment. Care must be taken at the venting hole of the furnace, which, left open, could dramatically alter the sintering temperature profiles. This was a problem that was discovered later, after some syntheses gave improper results. It was solved with a piece of alumina cotton, blocking the air currents yet leaving the generated overpressure out. The sintering temperature and duration must be correlated with the formation energy/atom of the various compounds in order for these not to segregate in different phases. The ones with lower energies of formation tend to segregate, and, as such, instead of having only one homogeneous crystalline structure, we obtain a mix of different oxidic compounds. The phase-diagram, if available, should be consulted, and also the solid-state diffusion constants of the constituents must be known.

**(A6) Methods: Characterization of the Samples***Devices used for characterization***Characterization by X-rays diffraction (XRD)**

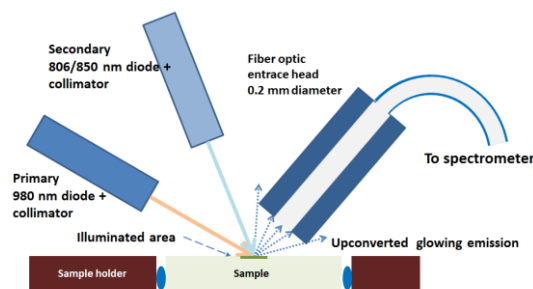
The X-rays used by the diffractometer are those from the characteristic radiation of Cu, specifically the Cu-K $\alpha_1$  line with the wavelength of 1.54056 Å. This line is generated by bombarding a Cu target with electrons in the 20-60 keV range and 5-100 mA current. All the XRD measurements were done with a Rigaku Miniflex II X-ray diffractometer from Tokyo, Japan.

**Characterization by Scanning Electronic Microscopy (SEM)**

Prior to the actual SEM investigation, the probes must be prepared in a specific way by first attaching them to a sample holder through a conductive adhesive tape. This sample holder will be inserted into a multiple samples rotating stage inside the microscope. Secondly, the probe is covered by an atomic layer of Au through argon plasma deposition. This helps the electrons to be scattered by the probe and form an image. Otherwise, they will be absorbed into the probe, and the image will be black. In order to investigate the atomic composition and check if the stoichiometry of the synthesized sample was the desired one, the Energy Dispersive X-ray Spectrograms (EDS) were measured. This is done by measuring the characteristic radiation of the elements in the sample, using the same electron beam used for the acquisition of SEM images, but in this case the sample revolver is tilted toward the EDS detector. All the SEM measurements were done with a microscope Tescan Vega 3LM from Brno, Czech Republic, equipped with a spectrometer for energy-dispersive X-ray spectroscopy (EDS).

*Photoluminescence spectra measurement*

The measuring of the upconversion spectra, a spectrometer from Ocean Optics (Orlando, FL, USA), USB4000CG-UV-NIR, was used. The software for driving the spectrometer was the OceanView version 1.6.7. This older version was proven to be better than the newer ones. The input in the spectrometer was through a special optical fiber with low absorption in the wavelength range of the spectrometer. The NIR diodes used were from the LCUXXE042Ap series and were driven with current control and power of emission control and inserted into the temperature-controlled bed. The thermal stabilization allowed to tune the IR wavelength with good precision (sub-nanometer) because the lasing wavelength varies with temperature. The collimation of the laser ray was done with a standard laser focuser, which was spotting on an area of around 0.5 mm<sup>2</sup>. This procedure permitted the probing of individual surface microcrystals. The fiber optic head, used for the gathering of the emitted signal, was positioned as closest from the illuminated spot (3 mm) in order to gather the maximum light, and the entrance diameter of the optical fiber was 200  $\mu$ m. **Figure at right** shows the relative positions of the NIR collimators, sample, and fiber optic entrance head of the spectrometer.

**(A7) Practical applications feasible in laboratory**

- **Wireless temperature monitoring** of industrial metallic parts during annealing or sintering. The system consists of oxidic upconverting minitargets distributed on the surface of the part, in the

places of interest. These mini targets are illuminated with lasers with the appropriate wavelengths and the UC response, which is temperature dependent, is measured. In this way, the thermal treatment process can be monitored without the need of expensive wire probes.

- **Displaying surfaces**. The device consists of a sticky plastic sheet, embedded with UC particles, sheet which is cut and stuck on different surfaces with different uses, signs, buttons, displays, drawing boards etc. This sheet is then illuminated with a laser beam with pulses according to a digitized image etc., and the instantaneous spots targeted by the laser starts to fluoresce.

- **E-ink style displays** made with UC particles. These particles could be tuned to emit in different colors and illuminated with a scanning NIR ray from a single laser diode. Very cheap displays can be done in this way.

- Screens made by **panels coated with a paint containing red/green/blue emitting oxides**, which are scanned with three appropriate excitation laser beams (UV range) whose pointing pixels are changed by rotating mirrors.

- **Battery level detector** by inserting  $\text{BaY}_2\text{O}_4\text{:Er:Yb}$  upconverting nano-particles at the anode and using the fact that  $\text{Li}^+$  ions, which are diffusing into the  $\text{BaY}_2\text{O}_4$  matrix, are altering the upconversion response of the UCNP.

- **Deformation sensors** which consist of thin sheets of dense crystalline ceramics (or even monocrystals) doped with Er:Yb. These sheets are glued on the surface whose deformation is to be measured and, upon illumination with 980 nm, the upconversion red/green emissions ratio is measured. Since the red/green ratio is dependent on Er-Yb ionic interdistance, the degree of deformation can be inferred.

## (A8) Studied compositions, methods of synthesis, targeted aspects

### Studied compositions (IA-B1).

Nr	Compound class	Composition	Designation
1	$\text{Y}_2\text{O}_3$ doped with Er, Yb	$\text{Y}_{1.98}\text{Er}_{0.02}\text{O}_3$	YO 1-0
2		$\text{Y}_{1.94}\text{Er}_{0.02}\text{Yb}_{0.04}\text{O}_3$	YO 1-2
3		$\text{Y}_{1.90}\text{Er}_{0.02}\text{Yb}_{0.08}\text{O}_3$	YO 1-4
4		$\text{Y}_{1.82}\text{Er}_{0.02}\text{Yb}_{0.16}\text{O}_3$	YO 1-8
5	$\text{BaGd}_2\text{ZnO}_5$ doped with Er, Yb	$\text{BaGd}_{1.98}\text{Er}_{0.02}\text{ZnO}_5$	BGZ 1-0
6		$\text{BaGd}_{1.94}\text{Er}_{0.02}\text{Yb}_{0.04}\text{ZnO}_5$	BGZ 1-2
7		$\text{BaGd}_{1.90}\text{Er}_{0.02}\text{Yb}_{0.08}\text{ZnO}_5$	BGZ 1-4
8		$\text{BaGd}_{1.82}\text{Er}_{0.02}\text{Yb}_{0.16}\text{ZnO}_5$	BGZ 1-8
9		$\text{BaGd}_{1.88}\text{Er}_{0.04}\text{Yb}_{0.08}\text{ZnO}_5$	BGZ 2-4
10		$\text{BaGd}_{1.80}\text{Er}_{0.06}\text{Yb}_{0.14}\text{ZnO}_5$	BGZ 3-7
11	$\text{BaLa}_2\text{ZnO}_5$ doped with Er, Yb	$\text{BaLa}_{1.94}\text{Er}_{0.02}\text{Yb}_{0.04}\text{ZnO}_5$	BLZ 1-2
12		$\text{BaLa}_{1.90}\text{Er}_{0.02}\text{Yb}_{0.08}\text{ZnO}_5$	BLZ 1-4
13	$\text{BaY}_2\text{ZnO}_5$ doped with Er, Yb	$\text{BaY}_{1.94}\text{Er}_{0.02}\text{Yb}_{0.04}\text{ZnO}_5$	BYZ 1-2
14		$\text{BaY}_{1.90}\text{Er}_{0.02}\text{Yb}_{0.08}\text{ZnO}_5$	BYZ 1-4
15	$\text{Y}_2\text{TiO}_5$ doped with Er, Yb	$\text{Y}_2\text{TiO}_5$	YTO 0-0
16		$\text{Y}_{1.98}\text{Er}_{0.02}\text{TiO}_5$	YTO 1-0
17		$\text{Y}_{1.98}\text{Yb}_{0.02}\text{TiO}_5$	YTO 0-1
18		$\text{Y}_{1.94}\text{Er}_{0.02}\text{Yb}_{0.04}\text{TiO}_5$	YTO 1-2
19		$\text{Y}_{1.90}\text{Er}_{0.02}\text{Yb}_{0.08}\text{TiO}_5$	YTO 1-4
20		$\text{Y}_{1.82}\text{Er}_{0.02}\text{Yb}_{0.16}\text{TiO}_5$	YTO 1-8
21		$\text{Y}_{1.88}\text{Er}_{0.04}\text{Yb}_{0.08}\text{TiO}_5$	YTO 2-4
22		$\text{Y}_{1.84}\text{Er}_{0.08}\text{Yb}_{0.08}\text{TiO}_5$	YTO 4-4
23		$\text{Y}_{1.88}\text{Er}_{0.06}\text{Yb}_{0.12}\text{TiO}_5$	YTO 3-6
24	$\text{BaY}_2\text{O}_4$ doped with Er, Yb	$\text{BaY}_{1.94}\text{Er}_{0.02}\text{Yb}_{0.04}\text{O}_4$	BYO 1-2
25		$\text{BaY}_{1.90}\text{Er}_{0.02}\text{Yb}_{0.08}\text{O}_4$	BYO 1-4
26	$\text{BaY}_2\text{O}_4\text{MgO}_5$ doped with Er, Yb	$\text{BaY}_{1.94}\text{Er}_{0.02}\text{Yb}_{0.04}\text{MgO}_5$	BYMO 1-2
27		$\text{BaY}_{1.90}\text{Er}_{0.02}\text{Yb}_{0.08}\text{MgO}_5$	BYMO 1-4

### Methods of synthesis of the samples (IA-B2).

Compound Class	Precursors	Method	Sintering
$\text{Y}_2\text{O}_3$ doped with Er, Yb	$\text{Y}(\text{NO}_3)_3 \cdot 6\text{H}_2\text{O}$ $\text{Er}(\text{NO}_3)_3 \cdot 6\text{H}_2\text{O}$ $\text{Yb}(\text{NO}_3)_3 \cdot 6\text{H}_2\text{O}$	coprecipitation precalcination 400 °C / 3h calcination 900°C / 3h	1300 °C / 4h



BaGd <sub>2</sub> ZnO <sub>5</sub> doped with Er, Yb	NaOH Gd(NO <sub>3</sub> ) <sub>3</sub> .6H <sub>2</sub> O Er(NO <sub>3</sub> ) <sub>3</sub> .6H <sub>2</sub> O Yb(NO <sub>3</sub> ) <sub>3</sub> .6H <sub>2</sub> O Zn(NO <sub>3</sub> ) <sub>2</sub> .6H <sub>2</sub> O Ba(CH <sub>3</sub> COO) <sub>2</sub> citric acid EDTA	citrate EDTA precalcination 400 °C /3h calcination 900°C / 3h	1250 °C / 3h
BaLa <sub>2</sub> ZnO <sub>5</sub> doped with Er, Yb	La(NO <sub>3</sub> ) <sub>3</sub> .6H <sub>2</sub> O Er(NO <sub>3</sub> ) <sub>3</sub> .6H <sub>2</sub> O Yb(NO <sub>3</sub> ) <sub>3</sub> .6H <sub>2</sub> O Zn(NO <sub>3</sub> ) <sub>2</sub> .6H <sub>2</sub> O Ba(CH <sub>3</sub> COO) <sub>2</sub> citric acid ethylene-glycol EDTA	sol-gel + EDTA precalcination 400 °C /3h calcination 900°C / 3h	1250 °C / 3h
BaY <sub>2</sub> ZnO <sub>5</sub> doped with Er, Yb	Y(NO <sub>3</sub> ) <sub>3</sub> .6H <sub>2</sub> O Er(NO <sub>3</sub> ) <sub>3</sub> .6H <sub>2</sub> O Yb(NO <sub>3</sub> ) <sub>3</sub> .6H <sub>2</sub> O Zn(NO <sub>3</sub> ) <sub>2</sub> .6H <sub>2</sub> O Ba(CH <sub>3</sub> COO) <sub>2</sub> citric acid ethylene-glycol EDTA	sol-gel + EDTA precalcination 400 °C /3h calcination 900°C / 3h	1250 °C / 3h
Y <sub>2</sub> TiO <sub>5</sub> doped with Er, Yb	Y(NO <sub>3</sub> ) <sub>3</sub> .6H <sub>2</sub> O Er(NO <sub>3</sub> ) <sub>3</sub> .6H <sub>2</sub> O Yb(NO <sub>3</sub> ) <sub>3</sub> .6H <sub>2</sub> O Ti butoxide ethylene-glycol citric acid	sol-gel precalcination 400 °C /3h calcination 900°C / 3h	1350 °C / 16h
BaY <sub>2</sub> O <sub>4</sub> doped with Er, Yb	Y(NO <sub>3</sub> ) <sub>3</sub> .6H <sub>2</sub> O Er(NO <sub>3</sub> ) <sub>3</sub> .6H <sub>2</sub> O Yb(NO <sub>3</sub> ) <sub>3</sub> .6H <sub>2</sub> O Ba(CH <sub>3</sub> COO) <sub>2</sub> citric acid ethylene-glycol EDTA	sol-gel + EDTA precalcination 400 °C /3h calcination 900°C / 3h	1200 °C / 3h
BaY <sub>2</sub> O <sub>4</sub> MgO <sub>5</sub> doped with Er, Yb	Y(NO <sub>3</sub> ) <sub>3</sub> .6H <sub>2</sub> O Er(NO <sub>3</sub> ) <sub>3</sub> .6H <sub>2</sub> O Yb(NO <sub>3</sub> ) <sub>3</sub> .6H <sub>2</sub> O C <sub>6</sub> H <sub>5</sub> O <sub>7</sub> .Mg <sub>1.5</sub> .9H <sub>2</sub> O Ba(CH <sub>3</sub> COO) <sub>2</sub> citric acid ethylene-glycol EDTA	sol-gel + EDTA precalcination 400 °C /3h calcination 900°C / 3h	1200 °C / 3h

*What aspects were targeted during the synthesis of the samples (IA-B3).*

The following aspects were targeted when synthesizing the oxidic compounds:

- low cost of precursor substances
- easiness and speed of the syntheses
- crystalline phases in the intermediary and final stages ( sharp peaks in XRD )
- no segregations of unwanted phases (no supplementary peaks other than the desired ones)
- low crystalline defects (seen in the positions of XRD peaks)
- high size of nanocrystals (seen in the width of the XRD peaks)
- homogeneity of compounds (uniform distributions seen in EDAX)
- uniform Er, Yb substitution (uniform distributions seen in EDAX)
- easiness of manipulation of the oxidic powders
- proper forming of the ceramic pellets, low porosity and cohesiveness
- homogeneity of the ceramic pellets (no variation in density)
- no internal defects in the ceramic pellets which could lead to breaks.
- no deformations of the pellets.
- good mechanical strength for manipulation, polishing and inserting into the measurement setup.

## (B0) Summary of the articles (original contributions)

### 1. MECHANISM FOR THE UPCONVERSION PROCESS FOR Y<sub>2</sub>O<sub>3</sub>:Er<sup>3+</sup>,Yb<sup>3+</sup> PHOSPHORS

This work reports the obtaining and characterization of Er, Yb co-doped yttria phosphors. The mechanism of energy transfer between dopant ions and upconversion of NIR photons by Er<sup>3+</sup> when sensitized by Yb<sup>3+</sup> is not fully understood. The study used yttrium, erbium, and ytterbium nitrates and sodium hydroxide to synthesize Er,Yb co-doped yttria powders. In the case of hydrothermal method,



aqueous solution of metal nitrates in appropriate molar ratio was first precipitated using aqueous solution of NaOH and then the reaction mixture was hydrothermally treated at 160 °C for 24 h. For obtaining Er, Yb co-doped yttria, a calcining step was required at 500 °C, 3h. The coprecipitation method involved the precipitation of the corresponding metal nitrates dissolved in water with a concentrated aqueous solution of NaOH, followed by an aging step of the reaction mixture at 60 °C for 20 h. Also, in this case, a calcining step was carried out at 800 °C for 3 hours. The resulting oxidic powders were then pressed and sintered at 1300 °C for 4 hours. Powders and sintered ceramic pellets were characterized using powder X-ray diffraction (XRD) and scanning electron microscopy (SEM), before and after calcination and sintering. Ceramic pellets were illuminated using a 976 nm laser diode with the NIR light emitted power of 50 mW.

The hydrothermal method produced acicular and tubular crystals with an average diameter of 1 μm and 10 μm length. After calcination at 500 °C, an yttria phase with cubic symmetry and a secondary Er<sub>2</sub>O<sub>3</sub> phase were identified, indicating the segregation of Er<sub>2</sub>O<sub>3</sub>. Hence, the photoluminescence spectra of Y<sub>2</sub>O<sub>3</sub>:Er,Yb phosphors obtained by co-precipitation route were measured. They showed a strong crystal field lifting the degeneracy of Er<sup>3+</sup> energy levels involved in the upconversion process. The thermal populating of <sup>2</sup>H<sub>11/2</sub> indicates a local temperature of around 57 °C. The phonon sideband is uniform only when Er<sup>3+</sup> ions are not sensitized by Yb<sup>3+</sup> ions. The presence of Yb<sup>3+</sup> ions significantly change phonon dispersion, promoting preferential directions in the crystal lattice. The study used the intense PL spectra for fitting, resulting in curves with a close superposition of measured data. The emission lines showed a complex structure of wavefunctions for energy levels and transitions. Line centers approximated the energy of individual Stark sublevels, with an accuracy of around 5 cm<sup>-1</sup>. Further refinements are needed to consider intensities, local symmetry group, and separation between electric and magnetic dipole transitions. Simulations were conducted for the free Er<sup>3+</sup> ion using average values for unsplit energy levels in the upconversion process. The chosen atomic parameter values were listed and the first 17 energy levels wavefunctions compositions, resulting from the simulations, were presented for the first time. Two observations were made: the energies determined in this work are lower than literature data, and the strong mixing of J manifolds contradicts the richness of the PL spectra, suggesting the simulation model is either limited or needs more input data. The presence of Yb<sup>3+</sup> ions significantly influences the efficiency of the upconversion process, with YO1-2 showing a sharp increase and YO1-4 reaching 8.3 times higher than YO1-0. Increasing Yb<sup>3+</sup> concentration leads to quenching effects, resulting in lower luminescence intensity in the visible domain. However, when Yb<sup>3+</sup> sensitizer ions are present, the red/green intensities ratio changes linearly with the logarithm of Yb<sup>3+</sup> concentrations, promoting red emission and increasing the likelihood of populating the <sup>4</sup>F<sub>9/2</sub> level.

This paper contributes to the understanding of the upconversion mechanism. It reveals that the intensity of visible upconversion spectra is highest in YO1-4, with Yb<sup>3+</sup> ions significantly influencing the process. The presence of Yb<sup>3+</sup> enhances the population of the <sup>4</sup>F<sub>9/2</sub> level of Er<sup>3+</sup>, increasing the probability of absorbing incident NIR radiation and transitioning to <sup>2</sup>G<sub>9/2</sub> level. This leads to the formation of the 415 nm line, and implying the existence of an intermediary energy level between <sup>4</sup>F<sub>9/2</sub> and <sup>4</sup>S<sub>3/2</sub>.

## 2. NONLINEARITY OF THE UPCONVERSION RESPONSE OF Er<sup>3+</sup> IN Y<sub>2</sub>TiO<sub>5</sub>:Er<sup>3+</sup>,Yb<sup>3+</sup> CERAMICS WHEN VARYING THE WAVELENGTH OF INCIDENT NIR EXCITATION RADIATION

The study investigated the UC efficiency of Er<sup>3+</sup> in near-infrared radiation using the Er<sup>3+</sup>:Yb<sup>3+</sup> activator-sensitizer pair. Using Y<sub>2</sub>TiO<sub>5</sub> ceramic doped with Er<sup>3+</sup> and Yb<sup>3+</sup>, the study revealed, for the first time, a nonlinear behavior in the UC process. The Y<sub>2</sub>TiO<sub>5</sub> matrix exhibited high sensitivity to the incident IR laser light, resulting in notable changes in spectral composition. This research could be useful in laser wavelength indicators, structural modifications, forgeries detection, and doppler sensors.

Er and Yb doped Y<sub>2</sub>TiO<sub>5</sub> powders were synthesized by Pechini method using erbium nitrate pentahydrate, ytterbium nitrate pentahydrate, yttrium nitrate hexahydrate, titanium(IV) n-butoxide 97%, citric acid, and ethylene glycol. The dopant concentrations were chosen to minimize lattice distortions. The resulting oxide powders were calcined at 900 °C for 3 h and were pressed and sintered at 1250 °C for 16 h.

The XRD analysis of oxides powder obtained at 900 °C revealed the formation of a single phase with cubic symmetry, while in the case of the sintered samples at 1250 °C for 16 h—was obtained the orthorhombic Y<sub>2</sub>TiO<sub>5</sub> phase with P1 symmetry with large voids potentially leading to lattice defects., High Yb<sup>3+</sup> concentrations resulted in fluorite Y<sub>2</sub>Ti<sub>2</sub>O<sub>7</sub> and hexagonal Y<sub>2</sub>TiO<sub>5</sub> formation because Yb<sup>3+</sup> has lower ionic radius than Y<sup>3+</sup>. SEM investigation revealed similar aspects of ceramics irrespective the concentration of dopants.

This study presents the upconversion emission of ceramics using grazing IR laser light at two wavelengths. The ceramics showed local variations in brightness due to the size of the crystals and uneven laser field. The study has a novel approach to the upconversion mechanism making the hypotheses that its sensibility is linked to detuning resonant energy transfer between Er<sup>3+</sup> and Yb<sup>3+</sup> ions. The high sensitivity of Er,Yb:YTO ceramics differs from other tested ceramics, showing similar upconversion spectra with linear dependence.

The upconversion spectra of Er,Yb:Y<sub>2</sub>TiO<sub>5</sub> ceramics revealed that phononic interactions influenced Er<sup>3+</sup> ion de-excitation. The UC of Y<sub>2</sub>TiO<sub>5</sub> was weak when only Er<sup>3+</sup> was present, but an increased efficiency was observed in the presence of Yb<sup>3+</sup> ions. The Lorentzian fitted peaks indicated that Er<sup>3+</sup> ions were trapped in a crystalline phase. The YTO 1-2 ceramic exhibited unique behavior, with an upconversion spectrum almost identical to Y<sub>2</sub>O<sub>3</sub> doped with 1% Er<sup>3+</sup> and 2% Yb<sup>3+</sup>. The upconversion efficiency for the Y<sub>2</sub>TiO<sub>5</sub> matrix is lower than that of Y<sub>2</sub>O<sub>3</sub> and increasing Yb<sup>3+</sup> concentration facilitates the transition from <sup>4</sup>F<sub>9/2</sub>→<sup>4</sup>I<sub>15/2</sub>.

An original idea was reported by analyzing the correlation between  $\text{Er}^{3+}$  and  $\text{Yb}^{3+}$  dopant distances in a cubic lattice of  $\text{Y}_2\text{TiO}_5$ . It founds that  $\text{Er}^{3+} \leftrightarrow \text{Er}^{3+}$  interaction must be considered for UC efficiency design. The study also measured photoluminescent integral intensities for green and red emission of IR laser radiation at different wavelengths. The output power saturates beyond 100 mW at 975.5 nm, indicating  $\text{Er}^{3+}$  ions prefer other decay channels or absorb photons, which is also an original hypothesis.

The emitted green-red intensities are not linear, and simulations showed quenching occurs when  $\text{Er}^{3+}$  is 4%, regardless of  $\text{Yb}^{3+}$  concentration. This sensitivity has practical engineering applications, including laser diode wavelength tuning and quality control.

### 3. COMPARISON BETWEEN UPCONVERSION RESPONSE OF $\text{Er}^{3+}$ SENSITISED WITH $\text{Yb}^{3+}$ IN VARIOUS OXIDIC CERAMIC HOSTS

This preprint paper presents, for the first time, a comparative assessment of the Er:Yb activator - sensitizer pair across ternary oxidic ceramics:  $\text{BaGd}_2\text{ZnO}_5:\text{Er},\text{Yb}$  (BGZ),  $\text{BaY}_2\text{ZnO}_5:\text{Er},\text{Yb}$  (BYZ),  $\text{BaLa}_2\text{ZnO}_5:\text{Er},\text{Yb}$  (BLZ),  $\text{Y}_2\text{TiO}_5:\text{Er},\text{Yb}$  (YTO), and  $\text{Y}_2\text{O}_3:\text{Er},\text{Yb}$  (YTO) used as reference material and shows the correlation between the increasing red emission intensity of  $\text{Er}^{3+}$  when  $\text{Yb}^{3+}$  concentrations increases, a fact not explained yet in the literature. Oxide powders were synthesized using either citrate-EDTA or Pechini techniques and calcined at 900 °C for 3 h. Then the resulting oxide powders were pressed as pellets and sintered at specific temperatures and durations.<sup>7</sup> The ceramic bodies were characterized by XRD and SEM. Visualizations of the crystal structures are provided.

The study focused on obtaining upconversion photoluminescent spectra of various  $\text{Er}^{3+}$ ,  $\text{Yb}^{3+}$  doped oxidic ceramics. The illumination power and spectra acquisition times were adjusted to achieve different emission intensities. BLZ had the smallest efficiency, while BYZ had the highest. The acquisition time was chosen to avoid saturation in the visible domain. The spectra showed a strong signal in the IR region of 950-1050 nm, indicating the sample dissipated the incident energy instead of upconverting it into higher energy photons. The percentage of red emission intensity increased with  $\text{Yb}^{3+}$  concentration, suggesting  $\text{Yb}^{3+}$  promotes the  $^4\text{F}_{9/2}$  level of  $\text{Er}^{3+}$ . The red intensity variation is linearly correlated with  $\text{Yb}^{3+}$  concentration, revealing energy transfers between  $\text{Er}^{3+}$  and  $\text{Yb}^{3+}$ . This comparative study presents, for the first time, detailed and superimposed UC spectra for different compounds, and can serve as a starting point for further research.

This study reveals, in a novel way, how the red component of  $\text{Er}^{3+}$  upconversion luminescence in oxidic ceramic hosts is enhanced with more sensitizer  $\text{Yb}^{3+}$  ions, while green emission decreases, and underlines, for the first time, how this behavior is consistent across all crystalline hosts, governed by the medium distance between  $\text{Er}^{3+}$  and  $\text{Yb}^{3+}$  ions. The average interionic distance depends on the concentrations of  $\text{Er}^{3+}$  and  $\text{Yb}^{3+}$ , which can be assessed through computer simulations. The study concluded that  $\text{Yb}^{3+}$  ions act as mirroring cavities, increasing the trapping efficiency of incoming 980 nm radiation. The upconversion spectra showed that red/green emission ratio increases linearly with the increase of the relative Yb:Er concentration, indicating that the  $\text{Yb}^{3+}$  ion sensitization effect on  $\text{Er}^{3+}$  ions is determined by interionic distance. The intensity of emissions was also compared. BYZ was the most efficient, with an intensity nearly four times higher than YO.

### 4. INTERIONIC DISTANCE DISTRIBUTIONS BETWEEN $\text{Er}^{3+}$ AND $\text{Yb}^{3+}$ AS DOPANTS IN SOME CRYSTAL MATRIX HOSTS USED FOR UPCONVERSION LUMINESCENCE

The red component of  $\text{Er}^{3+}$ 's upconversion emission is enhanced when  $\text{Yb}^{3+}$  ions are present, with increased concentrations, in oxidic ceramic samples doped with  $\text{Er}^{3+}$  and  $\text{Yb}^{3+}$ . This behavior is consistent across all crystalline hosts, regardless of their characteristics. This study reported how the average distances between  $\text{Er}^{3+}$  and  $\text{Yb}^{3+}$  ions governs this phenomenon, distances which are typically greater than the crystal's unit cell dimensions. Evaluating these average interionic distances is crucial for understanding the red shift phenomenon. The average dimensions of crystallite are considered, and a cube with 400 nm edges is used for the simulation. The crystalline matrix is filled with unit cells, and the positions of substituted ions are recorded in a list. The appropriate number of dopant ions for each concentration case is distributed using a random number generator. The distances to other dopants are calculated for each random position, and the arithmetic averages are built from these distances. The final averages list is used to assign the number of dopant ions with the closest  $n$  neighbors to the average distance in each interval.

As  $\text{Yb}^{3+}$  concentration increases, the distribution shifts towards lower values, with each  $\text{Er}^{3+}$  more surrounded by  $\text{Yb}^{3+}$ . The distributions are Poisson-like, with different parameters based on 3D spatial distributions and the specificity of the starting CIF data.

The abscissa value of a distribution peak indicates equal average radii for relative  $\text{Er}^{3+}$ - $\text{Yb}^{3+}$  concentration ratios of 1:2, 1:4, and 1:8, with  $R_{4^{1:2}}=R_{8^{1:4}}=R_{16^{1:8}}$ . For the first time, based on these distances, simple surrounding models can be built to estimate energy transfer between activator and sensitizer ions. The chosen neighboring unit cell depends on the maximal distribution of distances between  $\text{Er}^{3+}$  in the center and surrounding  $\text{Yb}^{3+}$ .

Simulations showed that red/green ratio intensities are directly linked to the number of  $\text{Yb}^{3+}$  sensitizer on a fixed-radius sphere.  $\text{Er}^{3+}$  ions interact with neighboring  $\text{Yb}^{3+}$  ions, forming a mirror with certain degrees of reflectivity. Phononic interactions remain constant regardless of concentration, as dopant ions do not strongly perturb the host crystal's phononic band structure.  $\text{BaGd}_2\text{ZnO}_5$  has higher upconversion efficiency than  $\text{Y}_2\text{O}_3$ , indicating that specific parameters of the host should be considered.

### 5. NONSTATIONARY BEHAVIOR OF THE UPCONVERSION PROCESSES OF $\text{Er}^{3+}:\text{Yb}^{3+}$ IONS PAIR DOPING THE $\text{Y}_2\text{O}_3$ CERAMIC ILLUMINATED WITH 976 NM LASER LIGHT

Illumination of  $\text{Y}_2\text{O}_3$  (YO) 1-2 pellets with IR laser light with 976 nm wavelength resulted in upconversion to visible range spectra. The ceramics were either heated to 70 °C and cooled to room temperature, or cooled at 0 °C and then warmed at room temperature (25 °C). The spectra were split into four parts, each corresponding to an emission from a specific transition. The purpose was to assess individual transition intensity and compare relative ratios in time. The experiment was purely evaluative, allowing for a better understanding of the phenomenon and it is for the first time when this kind of behaviour was reported. A FFT analysis of the oscillations for an interval of 300 seconds showed the highest amplitude at a frequency of 38.3 mHz. The upconversion intensity for  $^2\text{H}_{11/2}$  emission was found to be almost constant with temperature, with only  $^4\text{S}_{3/2}$  emission varying, which came as a surprise, since  $^2\text{H}_{11/2}$  is thermally populated from  $^4\text{S}_{3/2}$ .

The YO 1-2 sample was also monitored for 30 minutes at constant 30 °C, integrating all visible range (510-700 nm). The anti-Stokes band of  $\text{Yb}^{3+}$  was also monitored during this time interval, showing an almost constant integral during the monitoring. This proves that the variability in the upconverted emission is solely from the  $\text{Er}^{3+}$  ions interacting with the surrounding photon field, with a relatively high amplitude of variation, of about 20%, of the total emission.

The activator-sensitizer interaction is similar across host matrix types, and the effect could be a superposition of Rabi oscillations of an  $\text{Er}^{3+}$  ion surrounded by  $\text{Yb}^{3+}$ . The activator ions are trapped in cavities formed by  $\text{Yb}^{3+}$  sensitizers, and the cavity QED could explain the phenomenon and this is an original idea.

This oscillatory phenomenon could be useful in low-frequency generators, laser modulation, or thermally controlled burst signal generators.

## 6. THE EFFECT OF MgO INSERTION INTO THE INTERSTITIAL SPACES OF $\text{BaY}_2\text{O}_4$ ON THE UPCONVERSION RESPONSE OF $\text{Er}^{3+}:\text{Yr}^{3+}$ AT ILLUMINATION WITH 976 NM EXCITATION LIGHT

Crystalline materials with the general formula  $\text{BaLn}_2\text{ZnO}_5$  are studied for upconversion properties of  $\text{Er}^{3+}$  ions as dopants. The unit cells of  $\text{BaGd}_2\text{ZnO}_5$  (BGZ) and  $\text{BaY}_2\text{ZnO}_5$  (BYZ) have both similar orthorhombic structure. However, BYZ has a stronger upconversion emission intensity than BGZ due to different phonon frequencies in BYZ.

The study presents a new type of material  $\text{BaY}_2\text{O}_4$  with interstitial MgO. The energy of phonons affects the probability of multiphonon assisted transitions between energy levels of rare-earth ions. To increase efficiency in the UC process, the frequency of phonons must be controlled and decreased. To tweak phonon energies, the  $\text{Zn}^{2+}$  ion was replaced with a similar ion with +2 charge, colorless and having similar ionic radius for *penta* coordination.

The citrate-EDTA method was used to prepare  $\text{BaY}_2\text{O}_4\text{-MgO}$  and  $\text{BaY}_2\text{O}_4$  ceramics. The parameters were chosen to prevent  $\text{Y}_2\text{O}_3$  segregation from  $\text{BaY}_2\text{O}_4$ , as  $\text{Y}_2\text{O}_3$  has a lower energy of formation per mol.

The XRD patterns of BYO 1-2 and BYO-MgO 1-2 compared with the one simulated for  $\text{BaY}_2\text{O}_4$ , with inserted  $\text{Mg}^{2+}$  ions, aligned with the  $\vec{a}$  direction of the crystal, showed no traces of segregated MgO. This  $\text{BaY}_2\text{O}_4\text{-MgO}$  material is not reported in the literature and could have future applications. The  $\text{BaY}_2\text{O}_4$  unit cell, with Pnma-62 symmetry, has voids large enough to accommodate MgO, as shown in X-ray diffractograms. The crystal radius of  $\text{Mg}^{2+}$  is small enough to occupy these voids, making it a novel structure, as the literature and database lack data about it. Shown the upconversion spectra for BYO 1-2, BYO-MgO 1-2, and, for comparative purposes,  $\text{Y}_2\text{O}_3$  1-2, with  $\text{Y}_2\text{O}_3$  spectrum scaled down at 33% due to higher upconversion signal for the same illumination power.

The novelty of this study shows how MgO in BYO alters the phonon dispersion and up-conversion response of  $\text{Er}^{3+}$ , resulting in a lower UC efficiency for the same injected power. The  $\text{Yb}^{3+}$  anti-Stokes peaks show that while phonon energies are similar, the crystal field strength is higher in BYO and BYO-MgO.

## EOE (C) Conclusions YO - Conclusions

### *Conclusion drawn from the particular studies.*

Yttria ceramic doped with  $\text{Er}^{3+}$  and  $\text{Yb}^{3+}$  ions in various ratios and absolute percentages were obtained at 1300°C from the corresponding powders prepared by coprecipitation route. This method was found to be suitable for RE ions accommodation in the crystalline cubic lattice of the  $\text{Y}_2\text{O}_3$  host matrix.  $\text{Er,Yb}:\text{Y}_2\text{O}_3$  ceramics were utilized to investigate the upconversion (UC) process of incident NIR irradiation with 976 nm wavelength by  $\text{Er}^{3+}$  ions sensitized by  $\text{Yb}^{3+}$  ions, and a mechanism was suggested. The energy levels involved in the upconversion energy transfers were determined and the wavefunctions for the first 17 energy levels were computed. However, for more precision, the crystal field strength that causes the splitting of the Stark levels will be identified in future studies.

Erbium and ytterbium-doped yttrium titanate ceramics were obtained at 1250 °C using oxide powders prepared using the sol-gel method. SEM and XRD revealed that the microstructure and phase composition of doped  $\text{Y}_2\text{TiO}_5$  ceramics were very sensitive to dopant concentrations. When the  $\text{Yb}^{3+}$  concentration is increased, more hexagonal and fluorite phases formed, limiting the maximum  $\text{Yb}^{3+}$  concentration to 10% (mol).

The samples were irradiated at 973.5 and 975.5 nm and the resulting UC visible spectra were obtained and described. In the case of  $\text{Y}_2\text{TiO}_5:1\%\text{Er}^{3+},2\%\text{Yb}^{3+}$  it was noticed that the higher Stark level of  $^4\text{S}_{3/2}$  of  $\text{Er}^{3+}$  becomes more populated when illuminated with 973.5 vs. 975.5 nm, resulting in a significant shift in the hue and peak intensities in the UC response. In addition, the emitted green-red intensities, both relative and absolute, for the samples with other composition were measured and compared for the



973.5 and 975.5 nm irradiations, revealing significant differences that were not seen in other crystalline lattices tested or found in the literature.

The curves relating the emitted intensity to the excitation power of the incident radiation were not linear, with a saturation tendency above 100 mW for green (515-575 nm) in the case of 973.5 nm irradiation and red (640-700 nm) in the case of 975.5 nm illumination.

Simulations were run for the distributions of the interionic distances for  $\text{Er}^{3+} \leftrightarrow \text{Er}^{3+}$  and  $\text{Er}^{3+} \leftrightarrow \text{Yb}^{3+}$ , and the samples were ranked by the maximum distance for each dopant concentration.  $\text{Er}^{3+} \leftrightarrow \text{Er}^{3+}$  quenching occurs at 4%  $\text{Er}^{3+}$ , regardless of  $\text{Yb}^{3+}$  concentration, indicating that  $\text{Er}^{3+} \leftrightarrow \text{Er}^{3+}$  energy transfers are more common than those between  $\text{Er}^{3+}$  and  $\text{Yb}^{3+}$ . The upper Stark level of  $^4\text{S}_{3/2}$  is more populated when illuminated with 973.5 nm vs. 975.5 nm. This is puzzling because the difference between the two levels of  $^4\text{S}_{3/2}$ , split by the crystal field of  $\text{Y}_2\text{TiO}_5$ , is more than  $20 \text{ cm}^{-1}$ , which is the energy difference between 973.5 nm and 975.5 nm.

Further research will be conducted to determine the source of this energy difference; however, the effect's sensitivity necessitates precise engineering applications. Some of these are laser diode wavelength tuning, cheap laser diode quality control, laser wave-length indicators, crystalline structural modification indicators when YTO is incorporated in other bulk ceramics, cheap doppler sensors with under 2 nm precision detection for non-inertial optical fiber gyroscopes, and, finally, forgery prevention by including certain YTO nanodots in the protected samples.

A general comparison study was also performed on different types of oxide ceramic hosts with the same amounts of  $\text{Er}^{3+}$  and  $\text{Yb}^{3+}$ .

The upconversion spectra were measured for ceramics with Er:Yb dopant molar ratios of 1:2, 1:4, and 1:8, and the relative red/green percentage in total visible emission was plotted.

The comparison demonstrated, for the first time, that the proportion content of red vs. green emissions increases linearly with the logarithm of the relative Yb-Er concentration, a pattern that is consistent across the types of crystalline hosts. This finding unequivocally demonstrates that the  $\text{Yb}^{3+}$  ion sensitization impact on  $\text{Er}^{3+}$  ions is a phenomenon determined by interionic distance.

The intensity of the emissions under steady illumination was also measured and compared. BYZ was the most efficient, with an intensity nearly four times that of the reference, YO, whereas BLZ was comparable to YTO, with efficiency barely one-third that of YO.

An unusual behavior of the upconversion process of  $\text{Er}^{3+}$  was observed. The spectra were divided into the ranges with each range corresponding to the emission caused by the transition from the excited defined level of  $\text{Er}^{3+}$  to the ground state  $^4\text{I}_{15/2}$ .

The integral for each range, i.e., the intensity of the respective emissions, was measured at 50 ms intervals, and data points were collected for up to 1200 seconds.

Initially, the intensities were intended to remain constant over time; nevertheless, they oscillated. To further investigate this behavior, the pellets were heated to  $70 \text{ }^\circ\text{C}$  or cooled to  $0 \text{ }^\circ\text{C}$  before being inserted into the measuring system, and the upconversion intensities were evaluated while cooling (warming) to room temperature, which was  $25 \text{ }^\circ\text{C}$ . The exact temperature of the samples was not measured; only their overall behavior was evaluated.

Cooling promotes upconversion, whereas heating opposes it via multiphonon nonradiative decays. It should be noticed that the intensity of the transition from  $^2\text{H}_{11/2}$ , GRNA (green emission from 516 to 544 nm), is practically constant with temperature, whereas only the intensity of  $^4\text{S}_{3/2}$  varies (GRNB from 544 to 568 nm), resulting in an exponential relationship between GRNA and GRNB, as it should be because  $^2\text{H}_{11/2}$  is thermally populated from  $^4\text{S}_{3/2}$ . Why GRNA is nearly constant is a subject that future research will attempt to solve.

This oscillatory phenomenon has a variety of uses, including low-frequency generators, a low-cost way for modulating a laser in an outside control loop, and burst signal generators when higher frequencies are controlled.

Also, for the first time, a novel material was identified and used as a host for  $\text{Er}^{3+}$  ions.  $\text{BaY}_2\text{O}_4$  and  $\text{BaY}_2\text{O}_4\text{-MgO}$  ceramic doped with  $\text{Er}^{3+}:\text{Yb}^{3+}$  were obtained by pressing and sintering the metallic oxide mixture synthesized by sol-gel process.

The X-ray diffraction revealed that  $\text{BaY}_2\text{O}_4$  and  $\text{BaY}_2\text{O}_4\text{-MgO}$  have nearly identical X-ray diffractograms, with the  $\text{Mg}^{2+}$  ions well accommodated in the internal voids of  $\text{BaY}_2\text{O}_4$ .

Furthermore, the dopant ions were well accommodated into the matrix, replacing  $\text{Y}^{3+}$  ions with no evidence of additional phase segregation.

To the best of our knowledge, this is the first time the compound  $\text{BaY}_2\text{O}_4\text{-MgO}$  (BYMO) has been characterized, with no previous information available in the literature.

The samples were exposed to an NIR laser at 976 nm, and the upconversion emission spectra of  $\text{Er}^{3+}$  were measured.

The peaks in the spectra for BYMO 1-2 were less pronounced than those for BYO 1-2, indicating that  $\text{Mg}^{2+}$  ions reduce the efficiency of the upconversion by introducing new energy loss channels. The positions of the peaks, which are identical to those of  $\text{Y}_2\text{O}_3$ , indicate that the crystal field in  $\text{BaY}_2\text{O}_4$  and  $\text{BaY}_2\text{O}_4\text{-MgO}$  is as strong as that of  $\text{Y}_2\text{O}_3$ .

Furthermore, the anti-Stokes band of  $\text{Yb}^{3+}$  is consistent across all cases of BYO, BYMO, and  $\text{Y}_2\text{O}_3$ , showing an average phonon energy of  $620 \text{ cm}^{-1}$  for all of these oxidic ceramics. BYMO inhibits the emission of  $\text{Er}^{3+}$  from  $^4\text{F}_{9/2} \rightarrow ^4\text{I}_{13/2}$ , and  $\text{Mg}^{2+}$  ions placed in BYO are definitely the cause.

The mechanism by which Mg affects the UC of  $\text{Er}^{3+}$  in BYO will be investigated further, both experimentally and by studying the phonon dispersions in BYO and BYMO using ab-initio computing techniques.

Furthermore, it was established that  $\text{Er}^{3+}$  sensitization by  $\text{Yb}^{3+}$  is determined by their relative interdistance. These findings have the general application of fine-tuning the  $\text{Er}^{3+}$  UC response at 980 NIR by adjusting the Mg level in the BYO matrix. Another application would be to detect the presence and/or concentrations of  $\text{Mg}^{2+}$  ions that penetrate the BYO matrix and then compare the resulting UC spectrum to that of pure BYO.

RADI - Conclusion  
The behavior of increasing the red/green components ratio of the upconversion emission of  $\text{Er}^{3+}$  assisted by  $\text{Yb}^{3+}$ , when the concentration of the latter is increased, regardless of the host matrix of embedding, is due to interionic distances. As such, for the first time, simulations were done, which provided important insight into why the red (640-700 nm)/green (510-580 nm) ratio intensities are directly related to the number of  $\text{Yb}^{3+}$  sensitizers on a fixed-radius sphere, demonstrating that, at least at low concentrations,  $\text{Er}^{3+}$  ions interact with neighboring  $\text{Yb}^{3+}$  ions, forming a kind of mirror with varying degrees of reflectivity.

The phononic interactions should be the same, regardless of dopant concentrations, which were below 10%. This is because the dopant ions, which replace the  $\text{Gd}^{3+}$  or  $\text{Y}^{3+}$  ions in the lattice, do not significantly disturb the host crystal's phononic band structure.

Another reason is that dopant concentrations are insufficient to cause lattice deformations or structural alterations. Results show that  $\text{BaGd}_2\text{ZnO}_5$  has 20% bigger  $R_{4^{1:2}}, R_{8^{1:4}}, R_{16^{1:8}}$  radii than  $\text{Y}_2\text{O}_3$ , but the former is more efficient. This demonstrates that, in addition to average distances, the specific parameters of each crystalline host case should be considered when calculating the absolute value of upconversion efficiency (such as phonon energies or dielectric constant).

#### **Accents on the obtained results (IA-C1).**

*From the  $\text{Y}_2\text{O}_3$  study, the obtained results were:*

- finding an optimum method for synthesizing doped  $\text{Y}_2\text{O}_3$  and observing how sensitive is the final structure to the energy of formation of different crystalline phases.
- detailed characterization of the  $\text{Y}_2\text{O}_3$  upconversion spectra
- from the peaks positions were inferred the energy levels of  $\text{Er}^{3+}$  in  $\text{Y}_2\text{O}_3$
- coefficients of the wavefunctions were calculated
- the color distribution was correlated with  $\text{Yb}^{3+}$  concentration and
- a mechanism for upconversion was underlined and noted the necessity of the existence of an intermediary level between  $4S_{3/2}$  and  $4F_{9/2}$ .

*From the  $\text{BaGd}_2\text{ZnO}_5$ ,  $\text{BaY}_2\text{ZnO}_5$  and  $\text{BaLa}_2\text{ZnO}_5$  studies, the obtained results were:*

- finding the optimum method for synthesizing  $\text{BaLn}_2\text{ZnO}_5$  doped compounds
- observing the color distributions and intensities of the upconversion response of  $\text{Er}^{3+}$
- observe that the efficiencies are very different among compounds with the same stoichiometric formula, due to the differences between crystal unit cells
- observe how the density of the materials and the masses of the ions constituting the crystal unit cell influence the energy transfers among  $\text{Er}^{3+}$  levels.

*From the  $\text{Y}_2\text{TiO}_5$  study, the obtained results were:*

- finding the optimum method for synthesizing  $\text{Y}_2\text{TiO}_5$  doped compounds
- observe how the crystal unit cell is distorted by different concentration of dopants.
- observe the nonlinearity of the upconversion response of  $\text{Er}^{3+}$  to the illumination with NIR wavelengths with difference as small as 2 nm
- observe the strength of quenching between  $\text{Er}^{3+}$  ions demonstrating that the use of  $\text{Er}^{3+}$  concentrations greater than 2% is not efficient.
- observe the saturation effect in the UC emissions in the case of high  $\text{Yb}^{3+}$  concentrations demonstrating that too many sensitizers hinder the UC..

*From the study of the oscillatory behavior, the results were:*

- observing how the UC effect in  $\text{Y}_2\text{O}_3$  has a temperature dependence and also a nonstationary behavior, even if the exciting power is constant during time.
- this behavior very clearly hints to mechanisms of energy transfer which are not documented in literature and whose better understanding could lead to new discoveries and a better control of the  $\text{Er}^{3+}$  upconversion assisted by  $\text{Yb}^{3+}$ .

*From the interionic distance calculations study, the results were:*

- observing how the interionic distance distributions are behaving when varying the concentration of dopants in the various crystalline hosts
- demonstrating the fact that a geometric variation of the concentration of  $\text{Yb}^{3+}$  leads to same pattern of the variation of the influences that  $\text{Yb}^{3+}$  sensitizers have upon  $\text{Er}^{3+}$  and this correlate with the linear variation of red/green composition of UC spectra across all the samples observed.

*From the  $\text{BaY}_2\text{MgO}_5$  study, the results were:*

- finding the method of a good insertion of MgO in BYO by using Mg citrate instead of other Mg salts.
- the observation that Mg ions entering the interstices of BYO are altering the upconversion response of  $\text{Er}^{3+}$  and this is due to the phonon energies modifications
- identifying a modality to tune the phonon energies in a crystal and, by this, open a window to applications relying on this effect like thermal sensors or Mg concentration sensors.

## **(C) Dissemination**

### *Publications*



*ISI journals:*

- 1) Dudas, L.; Berger, D.; Matei, C. Mechanism for the upconversion process for  $\text{Y}_2\text{O}_3:\text{Er}^{3+},\text{Yb}^{3+}$  phosphors *U.P.B. Sci. Bull., Series B* (2023), 85(4)  
IF = 0.35
- 2) Dudaş, L., Berger, D., & Matei, C. (2024). Nonlinearity of the upconversion response of  $\text{Er}^{3+}$  in  $\text{Y}_2\text{TiO}_5:\text{Er}^{3+},\text{Yb}^{3+}$  ceramics when varying the wavelength of incident NIR excitation radiation. *Materials*, 17(16), 3994. <https://doi.org/10.3390/ma17163994>  
IF = 3.1

*Preprints:*

- 1) Dudaş, L. (2024). Interionic distance distributions between  $\text{Er}^{3+}$  and  $\text{Yb}^{3+}$  as dopants in some crystal matrix hosts used for upconversion luminescence. Pre-print. <https://doi.org/10.48550/arXiv.2409.17875> [cond-mat.mtrl-sci]
- 2) Dudaş, L., (2024). Comparison between upconversion response of  $\text{Er}^{3+}$  sensitised with  $\text{Yb}^{3+}$  in various oxidic ceramic hosts <https://doi.org/10.48550/arXiv.2410.02177> [cond-mat.mtrl-sci]
- 3) Dudaş, L., (2024). The effect of MgO insertion into the interstitial spaces of  $\text{BaY}_2\text{O}_4$  on the upconversion response of  $\text{Er}^{3+}:\text{Yb}^{3+}$  at illumination with 976 nm excitation light. <https://doi.org/10.48550/arXiv.2409.16568> [cond-mat.mtrl-sci]
- 4) Dudaş, L., (2024). Nonstationary behavior of the upconversion processes of  $\text{Er}^{3+}:\text{Yb}^{3+}$  ions pair doping the  $\text{Y}_2\text{O}_3$  ceramic illuminated with 976 nm laser light. <https://doi.org/10.48550/arXiv.2409.15921> [cond-mat.mtrl-sci]

*Poster presentations*

- 1) Dudaş, L., Enachi, A., Berger, D., & Matei, C. Analysis of Upconversion Luminescence in  $\text{Y}_2\text{O}_3:(\text{Er},\text{Yb})$  Phosphors Applications of Chemistry in Nanosciences and Biomaterials Engineering (NanoBioMat) 22 - 24 June 2022.
- 2) Dudaş, L., Relative interdistance distributions between  $\text{Er}^{3+}$  and  $\text{Yb}^{3+}$  dopant ions in some crystal matrix hosts used for upconversion luminescence Applications of Chemistry in Nanosciences and Biomaterials Engineering (NanoBioMat) 24 - 26 November 2022.
- 3) Dudaş, L., Nonstationary behaviour of the upconversion processes for the  $\text{Y}_2\text{O}_3$  ceramic doped with  $\text{Er}^{3+}:\text{Yb}^{3+}$  ions pair. Applications of Chemistry in Nanosciences and Biomaterials Engineering (NanoBioMat) 28 - 30 June 2023.

EOF

**(D) Personal contributions****1. Determination of the best synthesis methods for the oxidic compounds**

As physicist I managed to grasp the understanding of the intimate processes of the synthesis of the complex oxidic compounds by soft chemistry method, which involves the control of many parameters. Some of these are:

- Precision controlling of stoichiometry, which is very prone to errors even from the start of the experiments.
- Precise control of the solvents added
- Control of the synthesis parameters like temperatures and mixture stirring speeds.
- The continuous monitoring of the pH is paramount for a good complexation/chelation of the metallic ions.

The best method was found to be sol-gel, Pechini or citrate-EDTA method.

**2. Measurement setup - diode controller etc.**

I personally acquired the HR4000CG-UV-NIR spectrometer, made my own spectra measurement setup, sample holders, which allow for quick, safe, and clean manipulation of the samples, and probing the samples with pinpoint accuracy at microcrystal levels.

The NIR 980 nm laser diode controllers were made by myself, having current control loop, a power control loop, and a thermal control loop, permitted the subnanometer tuning of the laser emission, which allowed for the discovery of a new phenomenon.

None of this would have been possible at other more expensive and complex facilities because they lack the versatility that is now at my disposal.

**3. Performing calculations for determining the energy levels of  $\text{Er}^{3+}$** 

I personally acquired and configured the computer systems and the software used for the determination of the energy levels of  $\text{Er}^{3+}$  hosted in  $\text{Y}_2\text{O}_3$ , a task that is very time- and resource-consuming since it needs computing power because the parameter space beside being very large is not very smooth.

**4. Software for simulations of dopant distributions**

I realized the software for the simulations of the dopant distributions in bulk material, which helped me better understand the energy transfers between dopants and check the experimental evidence against the accepted theories. This work is in progress and is the base for future experiments and scientific papers.

**5. Found new phenomenon: the oscillatory behaviour of the upconversion process for  $\text{Er}^{3+}$** 

The spectrometer setup, which was realized in its entirety by myself, allowed me to discover the new phenomenon of the continuous oscillatory behavior of the upconversion.

This behavior is an important indication for the UC mechanism of the  $\text{Er}^{3+}$  sensitized by  $\text{Yb}^{3+}$ , which still is not clear after so many years and advances in the domain.

**6. Analyzed new material  $\text{Y}_2\text{TiO}_5$  with UC emission from  $\text{Er}^{3+}$  as dopant**

The same versatile spectrometer setup that allows for the fine tuning of the spectral line of the 980 nm laser diode allowed me to discover the nonlinear response of the upconversion of  $\text{Er}^{3+}$  when hosted in  $\text{Y}_2\text{TiO}_5$ , a material that was, anyway, not studied as a crystalline host for  $\text{Yb}^{3+}$  sensitized  $\text{Er}^{3+}$ . This new phenomenon could have important applications due to its finesse and sensitivity. As application examples I can indicate:

- counterfeit protection by embedding activated nanoparticles in the materials to be protected
- structural modifications of the materials by inserting doped  $\text{Y}_2\text{TiO}_5$  nanocrystals in the places of high stress.

## 7. Found new material BaY<sub>2</sub>MgO<sub>5</sub>

I synthesized BaY<sub>2</sub>MgO<sub>5</sub>, a material which is not documented, either at Materials Project or elsewhere, doped with Er<sup>3+</sup> and checked its UC spectrum. This host material was not characterized at all in the literature and will be the starting point for future research.

## 8. Extensive comparison of UC of Er<sup>3+</sup> as dopant in various oxitic crystalline materials

By comparing multiple spectra for the ceramic hosts studied, I showed that the common behavior of the red emission increases relative to the green emission one correlates with the Yb<sup>3+</sup> concentration across many host matrices.

This increase behavior has the same law of variation regardless of the host type, and I proposed to see how this behavior is correlated with the interionic distance between Er<sup>3+</sup> and Yb<sup>3+</sup>. This is the departure point for a theory of energy transfers between Er<sup>3+</sup> and Yb<sup>3+</sup>, which will be exposed in future publications.

## (E) References (shortened version)

- Zheng, B., Fan, J., Chen, B., Qin, X., Wang, J., Wang, F., Deng, R., & Liu, X. (2022). Rare-Earth doping in nanostructured inorganic materials. *Chemical Reviews*, 122(6), 5519–5603. <https://doi.org/10.1021/acs.chemrev.1c00644>
- Zhou, J., Liu, Q., Feng, W., Sun, Y., & Li, F. (2014). Upconversion Luminescent Materials: advances and applications. *Chemical Reviews*, 115(1), 395–465. <https://doi.org/10.1021/cr400478f>
- Bian, S., Lu, W., Zhou, L., & Jin, T. (2024). Advances in upconversion nanomaterials for tumor phototherapy. *Materials Today Communications*, 41, 110301. <https://doi.org/10.1016/j.mtcomm.2024.110301>
- Xu, J., Shi, R., Chen, G., Dong, S., Yang, P., Zhang, Z., Niu, N., Gai, S., He, F., Fu, Y., & Lin, J. (2020). All-in-One Theranostic Nanomedicine with Ultrabright Second Near-Infrared Emission for Tumor-Modulated Bioimaging and Chemodynamic/Photodynamic Therapy. *ACS Nano*, 14(8), 9613–9625. <https://doi.org/10.1021/acsnano.0c00082>
- Shwetabh, K., Banerjee, A., Poddar, R., & Kumar, K. (2024). Assessment of NIR-triggered PEG-coated NaGdF<sub>4</sub>:Tm<sup>3+</sup>/Yb<sup>3+</sup> bio-compatible upconversion nanoparticles for contrast enhancement in OCT imaging and optical thermometry. *Biomedical Materials*, 19(5), 055001. <https://doi.org/10.1088/1748-605x/ad580b>
- 43 Jurga, N., Runowski, M., & Grzyb, T. (2024). Lanthanide-based nanothermometers for bioapplications: excitation and temperature sensing in optical transparency windows. *Journal of Materials Chemistry C*, 12(32), 12218–12248. <https://doi.org/10.1039/d3tc04716d>
- Li, C., Yang, D., Ma, P., Chen, Y., Wu, Y., Hou, Z., Dai, Y., Zhao, J., Sui, C., & Lin, J. (2013). Multifunctional upconversion mesoporous silica nanostructures for dual modal imaging and in vivo drug delivery. *Small*, 9(24), 4150–4159. <https://doi.org/10.1002/smll.201301093>
- Maji, S. K., Sreejith, S., Joseph, J., Lin, M., He, T., Tong, Y., Sun, H., Yu, S. W., & Zhao, Y. (2014). Upconversion nanoparticles as a contrast agent for photoacoustic imaging in live mice. *Advanced Materials*, 26(32), 5633–5638. <https://doi.org/10.1002/adma.201400831>
- Chatterjee, D. K., & Yong, Z. (2008). Upconverting nanoparticles as nanotransducers for photodynamic therapy in cancer cells. *Nanomedicine*, 3(1), 73–82. <https://doi.org/10.2217/17435889.3.1.73>
- Ju, T., & Li, Z. (2024). An updated review for performance Enhancement of solar cells by spectral modification. *Energies*, 17(17), 4492. <https://doi.org/10.3390/en17174492>
- Chen, Y., Zhang, D., Peng, Z., Yuan, M., & Ji, X. (2021). Review of research on the Rare-Earth Doped Piezoelectric Materials. *Frontiers in Materials*, 8. <https://doi.org/10.3389/fmats.2021.679167>
- Shang, H., Yang, D., & Li, D. (2024). Highly sensitive optical thermometer based on Li<sup>+</sup>-doped erbium ytterbium silicate films. *Sensors and Actuators a Physical*, 115834. <https://doi.org/10.1016/j.sna.2024.115834>
- 11 Lee, C., Wi, S., Jeong, M., & Lee, Y. (2024). Excitation-dependent luminescent and optical thermometric properties of ER<sup>3+</sup> and YB<sup>3+</sup> co-doped K5Y(P2O7)<sub>2</sub>. *Optical Materials*, 155, 115900. <https://doi.org/10.1016/j.optmat.2024.115900>
- Liu, S., Ming, H., Cui, J., Liu, S., You, W., Ye, X., Yang, Y., Nie, H., & Wang, R. (2018). Color-Tunable upconversion luminescence and multiple temperature sensing and optical heating properties of Ba<sub>3</sub>Y<sub>4</sub>O<sub>9</sub>:Er<sup>3+</sup>/Yb<sup>3+</sup> phosphors. *The Journal of Physical Chemistry C*, 122(28), 16289–16303. <https://doi.org/10.1021/acs.jpcc.8b04180>
- Li, X., Zhu, M., Li, Z., Zhang, X., Wang, Y., Hao, H., & Li, L. (2024). Multi-mode up-conversion emission of Tm@Yb@Er phosphors for color modulation and thermometry. *Journal of Alloys and Compounds*, 1003, 175715. <https://doi.org/10.1016/j.jallcom.2024.175715>
- Wang, H., Liu, S., Zhang, B., Zhao, J., Xing, M., Tian, Y., Luo, X., & Fu, Y. (2024). Simultaneous modulation of multicolor upconversion emission and thermal-sensing performance of Ba<sub>5</sub>Zn<sub>4</sub>Y<sub>8</sub>O<sub>21</sub> phosphors. *Journal of the American Ceramic Society*, 107(9), 5964–5980. <https://doi.org/10.1111/jace.19892>
- Wang, J., Zhou, H., Zhu, K., Ye, L., Yu, X., Zhang, J., & Wang, L. (2024). Enhanced optical temperature sensing performance based on dual emission centers of Y<sub>2</sub>O<sub>3</sub>: Yb<sup>3+</sup>, Tm<sup>3+</sup>, Ho<sup>3+</sup> upconversion phosphor. *Ceramics International*. <https://doi.org/10.1016/j.ceramint.2024.07.025>
- Yang, J., Zhang, C., Peng, C., Li, C., Wang, L., Chai, R., & Lin, J. (2009). Controllable Red, Green, Blue (RGB) and Bright White Upconversion Luminescence of Lu<sub>2</sub>O<sub>3</sub>:Yb<sup>3+</sup>/Er<sup>3+</sup>/Tm<sup>3+</sup> Nanocrystals through Single Laser Excitation at 980 nm. *Chemistry - a European Journal*, 15(18), 4649–4655. <https://doi.org/10.1002/chem.200802106>
- J, I., Huignard, A., Bérard, M., Nordin, M. N., Hernández, I., Curry, R. J., Gillin, W. P., & Cheetham, A. K. (2010). Oxide phosphors for efficient light upconversion: Yb<sup>3+</sup> and Er<sup>3+</sup> co-doped Ln<sub>2</sub>BaZnO<sub>5</sub> (Ln = Y, Gd). *Journal of Materials Chemistry*, 20(19), 3989. <https://doi.org/10.1039/c000127a>
- Zhou, B., Tang, B., Zhang, C., Qin, C., Gu, Z., Ma, Y., Zhai, T., & Yao, J. (2020). Enhancing multiphoton upconversion through interfacial energy transfer in multilayered nanoparticles. *Nature Communications*, 11(1). <https://doi.org/10.1038/s41467-020-14879-9>
- Drozdowski, A., Poelman, D., Runowski, M., Hemmerich, H., Rivera-López, F., & Grzyb, T. (2024). Unleashing the glow: upconverting nanoparticles recharge persistent luminescent materials – applications in 3D-printing and optical coding. *Journal of Materials Chemistry C*. <https://doi.org/10.1039/d4tc01692k>
- Zhu, M., Li, Z., Li, X., Zhang, X., Wang, Y., Hao, H., & Li, L. (2024). Construction of active-inert core-shell structured nanocrystals for broad range multicolor upconversion luminescence. *Scientific Reports*, 14(1). <https://doi.org/10.1038/s41598-024-57523-y>
- Berry, M. T., & May, P. S. (2015). Disputed mechanism for NIR-to-Red upconversion luminescence in NaYF<sub>4</sub>:Yb<sup>3+</sup>,Er<sup>3+</sup>. *The Journal of Physical Chemistry A*, 119(38), 9805–9811. <https://doi.org/10.1021/acs.jpca.5b08324>
- Yin, Z., Li, H., Xu, W., Cui, S., Zhou, D., Chen, X., Zhu, Y., Qin, G., & Song, H. (2016). Local field modulation induced Three-Order Upconversion enhancement: combining surface plasmon effect and photonic crystal effect. *Advanced Materials*, 28(13), 2518–2525. <https://doi.org/10.1002/adma.201502943>
- Liu, Y., Wang, D., Shi, J., Peng, Q., & Li, Y. (2013). Magnetic tuning of upconversion luminescence in Lanthanide-Doped bifunctional nanocrystals. *Angewandte Chemie International Edition*, 52(16), 4366–4369. <https://doi.org/10.1002/anie.201209884>
- Vetrone, F., Boyer, J., Capobianco, J. A., Spgehini, A., & Bettinelli, M. (2004). Significance of Yb<sup>3+</sup> concentration on the upconversion mechanisms in codoped Y<sub>2</sub>O<sub>3</sub>:Er<sup>3+</sup>, Yb<sup>3+</sup> nanocrystals. *Journal of Applied Physics*, 96(1), 661–667. <https://doi.org/10.1063/1.1739523>
- Rivera-López, F., Torres, M., & De Cos, G. G. (2021). Upconversion and cooperative luminescence in YBO<sub>3</sub>:Yb<sup>3+</sup>- Er<sup>3+</sup>. *Materials Today Communications*, 27, 102434. <https://doi.org/10.1016/j.mtcomm.2021.102434>
- Hu, J., Zhu, D., Guo, K., Duan, B., Wu, Y., Li, Y., Wang, F., Jin, W., & Ding, C. (2024). Huge enhancement in upconversion luminescence near-infrared emission of KYb(MoO<sub>4</sub>)<sub>2</sub>: Er<sup>3+</sup> phosphor by doping Y<sup>3+</sup> ions. *Ceramics International*. <https://doi.org/10.1016/j.ceramint.2024.06.027>
- Wang, X., Li, X., Zhang, Y., & Chen, B. (2024). A comparative study of optical properties and temperature sensing characteristics of YMO<sub>4</sub>: Er<sup>3+</sup> (M = Nb, Ta, V, P) phosphors. *Inorganic Chemistry Communications*, 112812.

30. K. C., V., Sarkar, M. I., & Kumar, K. (2024). Investigation of upconversion and photoacoustic properties of NIR activated Er<sup>3+</sup>/Yb<sup>3+</sup> doped [RE]VO<sub>4</sub> (RE = Y, Gd) phosphors for photothermal conversion applications. *New Journal of Chemistry*. <https://doi.org/10.1039/d4nj02530j>
31. Du, J., Wang, P., Li, Y., Lin, H., & Poelman, D. (2024). Manipulation of multimodal and multicolor luminescence via interplay of traps and rare earth emission centers in calcium tungstate. *Inorganic Chemistry*. <https://doi.org/10.1021/acs.inorgchem.4c02423>
32. Zhang, Y., & Chen, G. (2024). Multifunctional photon conversion materials for enhancing silicon solar cells. *Light Science & Applications*, 13(1). <https://doi.org/10.1038/s41377-024-01431-3>
33. Makumbane, V., Kroon, R. E., Yagoub, M. Y. A., Erasmus, L. J. B., Coetsee, E., & Swart, H. C. (2024). The role of thickness on the structural and luminescence properties of Y<sub>2</sub>O<sub>3</sub>:Ho<sup>3+</sup>, Yb<sup>3+</sup> upconversion films. *Scientific Reports*, 14(1). <https://doi.org/10.1038/s41598-024-68367-x>
34. Jin, X., Sun, P., Yang, W., Wang, Y., & Xiao, Z. (2024). Thermal enhancement of upconversion luminescence in Negative-Thermal-Expansion HO<sup>3+</sup>-Doped Yb<sub>2</sub>-XW<sub>3</sub>O<sub>12</sub> phosphors. *Journal of Electronic Materials*. <https://doi.org/10.1007/s11664-024-11303-6>
35. De, A., Dey, A. K., Samanta, B., Sur, S., Paul, S., Adalder, A., Das, S., & Ghorai, U. K. (2022). Upconversion luminescence and time decay study of Yb–Er-doped BaWO<sub>4</sub> nanophosphor. *Journal of Materials Science Materials in Electronics*, 33(12), 9641–9649. <https://doi.org/10.1007/s10854-021-07607-6>
36. Borges, F. H., Mauricot, R., Neumeyer, D., De Souza, V. D. S., Verelst, M., & Gonçalves, R. R. (2024). Yb<sup>3+</sup> concentration influence on NIR and upconversion emission and temperature sensing properties of Er<sup>3+</sup>/Yb<sup>3+</sup> co-doped Ta<sub>2</sub>O<sub>5</sub> particles. *Journal of Luminescence*, 273, 120642. <https://doi.org/10.1016/j.jlumin.2024.120642>
37. Hu, J., Duan, B., Wu, Y., Li, Y., Wang, F., Ding, C., & Jin, W. (2024). Intense red upconversion luminescence and optical thermometry of a novel Yb<sup>3+</sup>/Er<sup>3+</sup> co-doped Ba<sub>3</sub>Sc<sub>2</sub>WO<sub>9</sub> phosphor. *Materials Research Bulletin*, 171, 112633. <https://doi.org/10.1016/j.materresbull.2023.112633>
38. Hu, J., Li, Y., Wu, Y., Duan, B., Guo, K., Wang, F., Liu, T., Jin, W., & Ding, C. (2024). Strong red upconversion luminescence of Yb<sup>3+</sup>/Er<sup>3+</sup> co-doped Sc<sub>6</sub>WO<sub>12</sub> phosphor for optical thermometry. *Journal of Molecular Structure*, 1319, 139511. <https://doi.org/10.1016/j.molstruc.2024.139511>
39. Jung, K. Y., Min, B. H., & Kim, D. H. (2024). Enhanced upconversion luminescence in (Ti<sub>1-x</sub>Si<sub>x</sub>)O<sub>2</sub>:Er/Yb phosphors via optimization of calcination temperature and silicon content. *Ceramics International*, 50(19), 36782–36791. <https://doi.org/10.1016/j.ceramint.2024.07.064>
40. Singh, P., Modanwal, S., Mishra, H., & Rai, S. (2024). Upconversion, downshifting, quantum cutting and back energy transfer from Yb<sup>3+</sup> to Er<sup>3+</sup> in Er<sup>3+</sup>/Yb<sup>3+</sup> co-doped CaTiO<sub>3</sub> phosphor, intense NIR generation for communication. *Ceramics International*. <https://doi.org/10.1016/j.ceramint.2024.06.028>
41. Jiang, T., Wang, X., Ye, R., Hua, Y., Jin, X., Guo, W., Liu, G., Long, Z., Zhang, B., Bai, G., Zhang, J., & Xu, S. (2024). Effects of optically inert ions on up-conversion luminescence and temperature-sensing properties of Y<sub>2</sub>O<sub>3</sub>: Er<sup>3+</sup>/Yb<sup>3+</sup>/Tm<sup>3+</sup> phosphors. *Journal of Alloys and Compounds*, 1000, 175135. <https://doi.org/10.1016/j.jallcom.2024.175135>
42. Roy, A., Dwivedi, A., Mishra, H., & Rai, S. (2021). Host dependent upconversion, color tunability and laser induced optical heating via NIR excitation in Ho<sup>3+</sup>, Yb<sup>3+</sup> doped YXO<sub>4</sub> (X = V, Nb, Ta) phosphor materials: Application as a security tool and optical heater. *Materials Research Bulletin*, 145, 111568. <https://doi.org/10.1016/j.materresbull.2021.111568>
43. Singh, S., Kachhap, S., Sharma, M., & Singh, S. K. (2023). Enhancing the temperature sensing property of a Ca<sub>0.79-x</sub>BixEr<sub>0.01</sub>Yb<sub>0.2</sub>MoO<sub>4</sub> phosphor via local symmetry distortion and reduction in non-radiative channels. *RSC Advances*, 13(22), 14991–15000. <https://doi.org/10.1039/d3ra02929f>
44. Singh, P., Modanwal, S., Mishra, H., & Rai, S. B. (2023). Intense photoluminescence in CaTiO<sub>3</sub>:Sm<sup>3+</sup> phosphors, effect of co-doping singly, doubly and triply ionized elements and their applications in LEDs. *RSC Advances*, 13(33), 22663–22674. <https://doi.org/10.1039/d3ra04468h>
45. Dutta, J., Chakraborty, M., & Rai, V. K. (2023). Tm<sup>3+</sup>, Yb<sup>3+</sup>:Zn<sub>2</sub>TiO<sub>4</sub> near infrared to blue upconversion phosphors for anti-counterfeit applications. *RSC Advances*, 13(34), 23386–23395. <https://doi.org/10.1039/d3ra03238h>
46. Cheng, X., Luo, J., & Rosei, F. (2024). Photon upconversion tuning through energy migration in lanthanides sensitized nanoparticles. *Nano Materials Science*. <https://doi.org/10.1016/j.nanoms.2024.04.003>